2021-08-06

Immunoaffinity Monoliths for Multiplexed Extraction of Preterm Birth Biomarkers from Human Blood Serum in 3D Printed Microfluidic Devices

Haifa Mohammad Almughamsi
Brigham Young University

Immunoaffinity Monoliths for Multiplexed Extraction of Preterm Birth Biomarkers from Human Blood Serum in 3D Printed Microfluidic Devices

Haifa Mohammad Almughamsi

A dissertation submitted to the faculty of
Brigham Young University
in partial fulfillment of the requirements for the degree of

Doctor of Philosophy

Adam T. Woolley, Chair
John C. Price
Ken A. Christensen
Steven R. Goates

Department of Chemistry and Biochemistry

Brigham Young University

ABSTRACT

Immunoaffinity Monoliths for Multiplexed Extraction of Preterm Birth Biomarkers from Human Blood Serum in 3D Printed Microfluidic Devices

Haifa Mohammad Almughamsi
Department of Chemistry and Biochemistry, BYU
Doctor of Philosophy

Preterm birth (PTB) results in over 15 million early births annually and is the leading cause of neonatal deaths. There are no clinical methods currently available to evaluate risk of PTB at early stages in pregnancy; thus, a rapid diagnostic to analyze PTB risk would be beneficial. Microfluidic immunoaffinity extraction is a promising platform for preparing complex samples, such as maternal serum with PTB risk biomarkers. 3D printed microfluidic devices have advantages over conventional microfluidic systems including simple fabrication and potential for iterative optimization to improve designs. In this work, I developed immunoaffinity monoliths in 3D printed microfluidic devices modified with antibodies to enrich PTB biomarkers from human blood serum. I retained and eluted a peptide PTB biomarker in both buffer and blood serum using an immunoaffinity column. An additional three PTB biomarkers were also successfully extracted either from buffer or blood serum on single-antibody columns. Both polyclonal and monoclonal antibodies to PTB biomarkers were characterized by dot blots, biolayer interferometry, and surface plasmon resonance to determine their specificity and dissociation constants. I created multiplexed immunoaffinity columns to simultaneously enrich three PTB biomarkers from depleted human blood serum in a single extraction. This is the first demonstration of multiplexed immunoaffinity columns for PTB biomarkers in a 3D printed microfluidic device. My work is a key step towards the future development of 3D printed microfluidic devices for rapid PTB testing.

Keywords: preterm birth (PTB), laser induced fluorescence (LIF), porous polymer monolith, multiplexed antibodies, immunoaffinity extraction, 3D printing, point of care (POC)

ACKNOWLEDGMENTS

First, I thank God for paving the way for me to achieve this milestone, and then my special gratitude to my lovely husband, Yousef Alharbi for making this success possible, for his unconditional support and motivation until the end of this journey. He boosts my energy to reach this goal while he is pursuing his own studies in the business management field. I also would like to thank my kids, Leen, Haneen, and Hattan, who have been my motivation and inspiration, for their sacrifice during this journey.

I am so grateful for my dad, sisters, brothers, extended family, neighbors, and friends for their consistent support, prayers, and words of wisdom. Special thanks to my advisor Dr. Adam Woolley for his assistance during the challenges that came on my way, and for valuable feedback, and expertise that I gained working under his supervision. This thanks also continues to my committee members Dr. John Price, Dr. Ken Christensen, and Dr. Steven Goates for their efforts, time, and advice, and for helping me become a critical thinker. I also thank my lab mates for listening to me when I bounce ideas: Ellen Parker, Anna Bickham, Mike Beauchamp, Jacob Nielsen, Joule Esene, Robert Hanson, Basu Aryal, Dulashani Ranasinghe, Yesman Akuoko, Chao Pang and many others.

Special thanks to Dr. Kelsey Budge, Dr. Santosh Misal, and Dr. Jeremy Tsang for their time and effort to listen to my research and suggestions. I also thank my country, Saudi Arabia, for a scholarship, and the College of Science at Taif University for funding me to complete this path. I thank Brigham Young University and the Department of Chemistry and Biochemistry for allowing me to use their facilities.

TABLE OF CONTENTS

LIST OF TABLES

LIST OF FIGURES

1. INTRODUCTION

1.1 Preterm Birth

Preterm birth (PTB) is birth prior to 37 weeks of pregnancy. It is the most common type of pregnancy complication with an incidence rate of 1 out of every 9 births in the United States.[1-4] PTB is also a contributing cause in most neonatal deaths. PTB infants can have multiple problems through their lives including hearing and vision loss, acute respiratory failure, behavioral problems, sensory difficulty, and chronic lung disease.[5] A variety of causes have been investigated, but in the majority of PTB cases no specific cause is found. Thus, there is a major need for an inexpensive and rapid diagnostic method that can accurately evaluate the risk of PTB at an early stage of pregnancy.

Nine PTB biomarkers were identified that show significant predictive power for the onset of early labor as seen in Table 1.1.[1] These biomarkers found in maternal blood serum include four previously known proteins: ferritin, lactoferrin, thrombin-antithrombin complex, and tumor necrosis factor-receptor type 1; and two peptides: corticotropin-releasing factor and defensin. Furthermore, Esplin and collaborators[1] have discovered three additional serum peptide biomarkers. Peptides 1-3 are fragments of a larger protein called inter-alpha-trypsin inhibitor heavy chain 4 (ITIH4). This panel of nine maternal serum biomarkers allows for PTB prediction with 90% selectivity and 80% specificity.

Table 1.1 PTB biomarkers.

PTB Biomarker	Abbreviation	Normal Level (nM)	PTB Risk Level (nM)
PTB Peptide 1	P1	*	*
Corticotropin Releasing Factor	CRF	0.06	0.075
PTB Peptide 2	P2	*	*
PTB Peptide 3	P3	*	*
Defensins	Def	*	130
Tumor Necrosis Factor-α Receptor Type 1	TNF	0.05	0.06
Lactoferrin	LF	6	3
Thrombin-Antithrombin III	TAT	7500	4900
Ferritin	Fer	0.02	0.040

*Level is not known

1.2 Biomarker Analysis

Several approaches are available for clinical biomarker analysis including liquid chromatography,[6] enzyme-linked immunosorbent assay (ELISA),[7] and mass spectrometry.[6] These bioanalytical methods can achieve reliable results, but are expensive, time-consuming, and not portable. Additionally, these approaches require many sample preparation steps and an experienced technician to generate accurate results.

Liquid chromatography coupled with mass spectrometry (LC-MS) offers selective and sensitive analysis for a variety of biomarkers.[6] However, the sample preparation steps prior to LC-MS limit the success of this technique for analysis of multiple biomarkers.[8] Esplin and collaborators[1] purified PTB peptides from serum proteins using sample precipitation to access the low molecular weight proteome prior to LC-MS analysis. All these intensive steps hinder biomarker quantification.

ELISA is a robust technique that is widely used in clinical biomarker analysis, though challenges exist for multiplexing.[7] Sandwich immunoassay can measure proteins due to the multiple epitopes available, but peptides must be detected by competitive immunoassay due to

their small size.[9] Both these assays are still limited by difficulties in multiplexing and lower sensitivity and specificity for competitive immunoassay. Both LC-MS and ELISA are not ideal options to analyze this combined panel of serum proteins and peptides related to PTB. Thus, an improved analysis method for PTB biomarkers is needed.

1.3 Microfluidics

Microfluidics involves controlling and manipulating liquids at the sub microliter scale.[10] The small volumes of liquid are passed through tiny channels in a device often called a lab-on-a-chip[11] where they can react, be analyzed, or manipulated.

Due to their micro-scale dimensions (<100 μm), microfluidic devices offer multiple advantages over conventional laboratory techniques. Microfluidic devices use lower volumes of sample and reagents, making this technology ideal for handling costly or toxic reagents.[12] Moreover, the small size of microfluidic devices results in faster analysis times, better temperature control, lower energy consumption, and portability.[11] All these benefits make microfluidic devices a promising platform for sensitive and cheap analysis of PTB biomarkers.

Originally, microfluidic devices were fabricated in silicon or glass using photolithography. This fabrication technique requires multiple processes, such as patterning, bonding, and etching steps.[13,14] All these processes are costly and complicate device fabrication, so alternative techniques to overcome these limitations are needed.[15]

1.4 3D Printing

Three-dimensional (3D) printing is an additive manufacturing process that creates 3D objects layer by layer using a computer designed file.[16] 3D printing has numerous advantages over traditional microfabrication including lower costs, fewer toxic chemicals, and increased portability because it does not require use of a cleanroom environment.[17,18] These features make

3D printing useful in many applications like dentistry and the aerospace industry to create precise models, prototypes, and patterns.[19] Recently, 3D printed microdevices have received attention due to the wide variety of benefits this technique offers such as rapid, iterative optimization where experimental data can provide feedback to improve design.[20]

Stereolithography (SLA) is one type of 3D printing which uses a liquid resin that is photopolymerized one layer at a time by exposure to UV light. A customized SLA 3D printer built by Nordin's group[20] at BYU has been used to make 20 μm × 20 μm channels in complex fluidic patterns, and Gong et al.[21,22] showed that pumps and valves can be 3D printed for microfluidic channels providing a pressure driven system.

Microfluidic channels can also be 3D printed and used for PTB biomarker analysis.[23] Parker et al.[24] developed an immunoaffinity monolith in 45 μm × 50 μm cross section microfluidic channels in a 3D printed microfluidic device to purify ferritin from human blood serum. Bickham et al.[25] adapted this design to polymerize a solid-phase extraction monolith to retain and elute this panel of nine PTB biomarkers. Creating microfluidic channels in a 3D printed device is possible, and when coupled with monolithic columns, will significantly advance the field of biomarker isolation and identification.

1.5 Monoliths

A monolith is a porous polymer, which has been researched for more than two decades resulting in the development of many applications.[26] Monolithic columns are used in chromatography applications and fabricated from multiple materials such as silica or polymers.[27] Monoliths allow in situ polymerization[24-25,28] and can be formulated to have a high flow rate, reduced mass transfer resistance, and low backpressure compared to traditional packed bead columns.[27] Affinity monoliths can be created by using different microfluidic channel materials to

retain analytes on the antibody column.[24,29]

An immunoaffinity monolith uses reactive monomer, glycidylmethacrylate (GMA), a cross linker like ethylene dimethacrylate (EDMA), porogens like cyclohexanol and dodecanol, and a photoinitiator.[24,29] These components are well researched, commercially available, and easy to prepare. The monomer and cross linker determine the properties of the monolith, such as the polarity, and polymerized structure. The crosslinker also determines the rigidity and pore size of the monolith. The porosity and surface area of the monolith can be controlled by adjusting the ratio of the porogens in the monolith formulation.

The GMA monolith surface can be functionalized to immobilize the target. For instance, antibodies can be covalently immobilized to a GMA column in one step by an epoxy group[24] or in multiple steps by the Schiff base method.[30] After antibody binding, the biomolecule of interest passes through the column and binds specifically to its target. Then, rinsing buffer is applied to remove weakly bound or non-retained analytes. Next, the elution buffer is flowed through the column and the biomolecule dissociates from its target. Immunoaffinity monoliths methods are widely used to retain analytes in a column via immobilized antibodies.

Several other methods and applications of affinity monoliths are also reported. Knob et al.[31] developed affinity monoliths modified with oligonucleotides and polymerized in a microfluidic device to capture DNA for sepsis diagnosis. Monoliths can be easily created inside a microchannel, offering a useful support for many applications.

1.6 Immunoassays

An immunoassay is a biochemical technique commonly used in biomarker analysis[14] to detect a target analyte in a mixture through a high affinity antibody. It works by binding of an antibody to a solid surface, which an antigen is then flowed over. This allows for the formation

of antibody-antigen complex. The ability of the antibody to recognize a specific antigen is necessary as it allows analysis of a range of analytes. The work described in this dissertation focuses on measuring multiple PTB biomarkers after they bind to their target antibodies on an affinity monolith. The enrichment of these biomarkers will make use of immunoaffinity monoliths in a simple 3D printed microfluidic chip possible.

1.6.1 Immunoassays in Microfluidics

Immunoassays in microfluidics are advantageous due to the low volume required, the ease of use, and potential for automation.[12] Developing an immunoassay in a microfluidic device further has the ability to provide a point of care analysis platform.

1.6.2 Antibodies

Antibodies are glycoproteins that have high selectivity and specificity toward their binding target. Antibodies are widely used in microfluidic immunoassays.[24,32] They have the capability to be immobilized on several support types. For instance, antibodies can be immobilized in a porous monolith inside a microfluidic channel, or on beads, or nanoparticles.[24,29, 33-34]

Antibodies are composed of four polypeptide chains (two heavy and two light polypeptide chains) and form a "Y" shape as seen in Figure 1.1. The polypeptide chains are connected to each other by disulfide bonds. Each arm of "Y" called the Fab region, contains an antigen binding site that recognizes an epitope on a specific antigen. This region contains one constant and one variable domain from each (heavy and light) chain of the antibody. The base of the "Y" is called the Fc region and contains two heavy chains. Polyclonal and monoclonal antibodies are the main antibody types used in immunoassay.

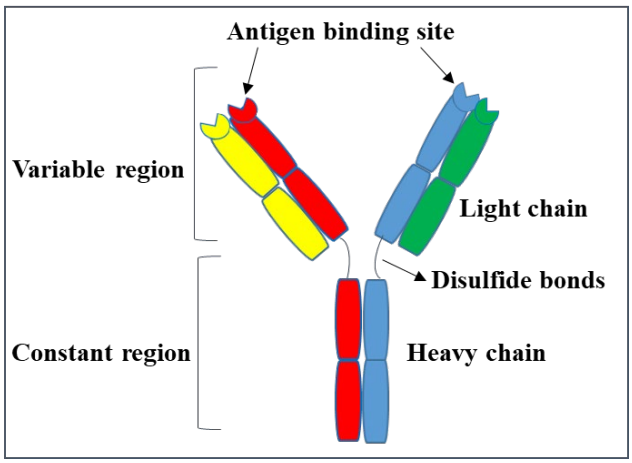

Figure 1.1: Diagram of an antibody**.**

1.6.2.1 Monoclonal and Polyclonal Antibodies

Antibodies used in immunoassay are monoclonal and polyclonal, and each type has its own pros and cons. Monoclonal antibodies are homogenous. They are produced from a single B cell; therefore, they recognize only one specific epitope of the antigen. Monoclonal antibodies have low cross reactivity with other proteins but are expensive to produce.[35]

Polyclonal antibodies are heterogeneous. They are made from multiple B cells and are easier to produce than monoclonal antibodies. Polyclonal antibodies are able to recognize different epitope sites in the same antigen.[35] Because polyclonal antibodies recognize many different epitopes on a single antigen, cross reactivity is more common in this antibody type.[36] Polyclonal antibody specificity is also reduced compared to a monoclonal antibody.

1.6.2.2 Dot Blot

A dot blot is a simple, yet powerful molecular biology technique, performed to determine an antibody's compatibility toward specific antigens. The dot blot process is a straightforward method where the antigens of interest are dotted on a nitrocellulose membrane. Then, the membrane is blocked to prevent non-specific binding. After blocking, the membrane is rinsed

and the target antibody is incubated to bind to its antigen. Next, a secondary antibody is incubated for fluorescence detection. Last, the membrane is scanned to determine whether the antigen and antibody are compatible, indicated by presence of fluorescence dots.

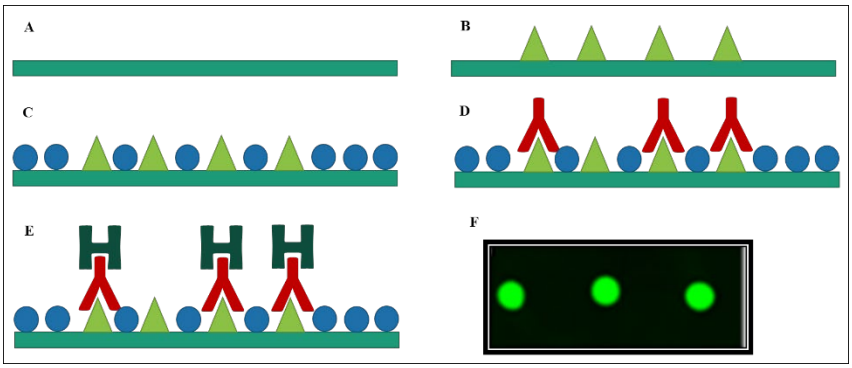

Figure 1.2 Dot blot process. A) Nitrocellulose membrane. B) PTB biomarker dots. C) Blocking agent applied (blue). D) Primary antibody added (red). E) Secondary antibody applied (dark green). E) Dot blot image after scanning.

1.7 Biolayer Interferometry and Surface Plasmon Resonance

Biolayer interferometry (BLI) and surface plasmon resonance (SPR) are widely used optical biosensing techniques that measure biomolecular interactions.[37-39] BLI analyzes the interference patterns of white light reflected from two surfaces. The first surface has immobilized proteins on the biosensor tip, whereas the second surface is an internal reference layer from the instrument. Binding between the analyte in the solution and the ligand immobilized on the biosensor tip causes an increase in the optical thickness, which leads to a wavelength shift and thus a change in the interference which is measured in real time. In SPR, one binding partner is attached to the surface of the sensor tip while the other partner is injected in continuous flow.[40] SPR measures changes in the intensity of light reflected at a specific angle from the glass side of the sensor surface. When a molecule binds to the sensor surface, the refractive index near the surface changes, which alters the angle of minimum reflected intensity. The change in SPR angle

is proportional to the mass of material bound. Both BLI and SPR assays have the ability to measure binding specificity and rate of association and dissociation with high precision and accuracy.[40]

1.7.1 Dissociation Constant (K_d)

Binding affinity between a biomolecule and its target can be assessed by the equilibrium dissociation constant (K_d). High binding affinity between an antigen and its target is indicated by a lower K_d value, while a higher K_d value shows lower binding affinity between antigen and target. Understanding the kinetics of the interaction between each biomarker and its target antibody can help to distinguish between retention of different biomarkers when multiple antibodies are attached to an immunoaffinity column.

1.8 Dissertation Overview

In this dissertation, I describe the development of 3D printed microfluidic devices for early detection of PTB risk. The devices contain an affinity monolith that is antibody modified, which will allow me to extract PTB biomarkers. This work shows the ability to purify multiple PTB biomarkers from human blood serum in 3D printed microfluidic devices.

Chapter 2 describes the development of immunoaffinity monoliths to extract the PTB peptide biomarker corticotropin releasing factor (CRF) from human blood serum in a 3D printed microfluidic device. Successful retention and elution of CRF is achieved in both buffer and blood serum from the anti-CRF column. This work is the first demonstration of PTB peptide extraction by an immunoaffinity column in a 3D-printed device. This is a significant step towards the analysis of a panel of PTB biomarkers in human blood serum as part of a PTB risk diagnostic.

Chapter 3 demonstrates the characterization of antibodies targeting PTB biomarkers. Selective binding between PTB biomarkers and off-target antibodies is demonstrated. Immunoaffinity extraction of the following individual PTB biomarkers, ferritin, lactoferrin and peptide 2, in 3D printed microfluidic devices is reported. This chapter also describes the binding affinity, or dissociation constant, for PTB biomarkers toward their targeted antibodies. The dissociation constants reported in this chapter are for polyclonal antibodies toward several of the PTB biomarkers. This work provides a promising foundation for extraction of multiple PTB biomarkers on immunoaffinity columns.

Chapter 4 shows the successful development of multiplexed immunoaffinity monoliths for extraction of multiple PTB biomarkers, CRF, TNF, and TAT from depleted human blood serum in 3D printed devices. A GMA monolith was modified with multiple antibodies to extract and enrich the PTB biomarkers from human blood serum. The equilibrium dissociation constant for each monoclonal antibody toward its target PTB biomarker was determined. PTB biomarker retention conditions were optimized for successful extraction. The PTB biomarkers were then selectively retained on these multiplexed antibody columns. This work yields promising steps towards purifying all nine PTB biomarkers from human blood serum as an important process in a complete diagnostic.

Chapter 5 summarizes the work in this dissertation and provides insightful suggestions for future directions to advance the work for PTB risk detection with 3D printed microfluidic devices.

1.9 References

1. Esplin, M. S.; Merrell, K.; Goldenberg, R.; Lai, Y.; Iams, J. D.; Mercer, B.; Spong, C. Y.; Miodovnik, M.; Simhan, H. N.; van Dorsten, P.; Dombrowski, M. Proteomic identification of serum peptides predicting subsequent spontaneous preterm birth. *Am. J. Obstet Gynecol.* **2011,** *204*, 391 e1-8.

2. Blencowe, H.; Cousens, S.; Chou, D.; Oestergaard, M.; Say, L.; Moller, A. B.; Kinney, M.; Lawn, J. Born Too Soon: The global epidemiology of 15 million preterm births. Reprod. *Health*. **2013,** *10*, S2.

3. Centers for Disease Control and Prevention. Reproductive Health: Preterm Birth. https://www.cdc.gov/reproductivehealth/maternalinfanthealth/pretermbirth.htm (accessed October 30, **2020**.

4. Rush, R. W.; Keirrse, M. J. N. C; Howat, P.; Baum, J. D.; Anderson, A. B. M.; Turnbull, A. C. Contribution of preterm delivery to prinatal mortality. *Br. Med. J.* **1976,** *2,* 965-968.

5. Institute of Medicine of the National Academies. Preterm Birth: Causes, Consequences, and Prevention. IOM, Wahington, DC, **2007**.

6. Gillette, M. A.; Carr, S. A. Quantitative analysis of peptides and proteins in biomedicine by targeted mass spectrometry. *Nat. Methods.* **2013,** *10* (1), 28-34.

7. Tighe, P. J.; Ryder, R. R.; Todd, I.; Fairclough, L. C. ELISA in the multiplex era: potentials and pitfalls. *Proteomics. Clin. Appl.* **2015,** *9*, 406-22.

8. Novakova, L.; Vlckova, H. A review of current trends and advances in modern bio-analytical methods: chromatography and sample preparation. *Anal. Chim. Acta.* **2009,** *656*, 8-35.

9. Lim, S. L.; Lchinose, H.; Shinoda, T.; Ueda, H. Noncompetitive Detection of Low Molecular Weight Peptides by Open Sandwich Immunoassay. *Anal. Chem.* **2007,** *79, 6193-6200.*

10. Xie, Z.; Pu, H.; Sun, D. W. Computer simulation of submicron fluid flows in microfluidic chips and their applications in food analysis. *Compr. Rev. Food. Sci. Food. Saf.* **2021,** DOI:10.1111/1541-4337.12766

11. Pandey, C. M.; Augustine, S.; Kumar, S.; Kumar, S.; Nara, S.; Srivastava, S.; Malhotra, B. D. Microfluidics Based Point-of-Care Diagnostics. *Biotechnol. J.* **2018,** *13* (1), 1700047.

12. Chin, C. D.; Linder, V.; Sia, S. K. Commercialization of microfluidic point-of-care diagnostic devices. *Lab Chip* **2012,** *12* (12), 2118-34.

13. McDonald, J. C.; Duffy, C. D.; Anderson, J. R.; Chiu, D. T.; Wu, H.; Schueller, O. J. A.; Whiteside, G. M. Fabrication of microfluidic systems in poly(dimethylsiloxane). *Electrophoresis.* **2000,** *21* (27-40).

14. Yang, W.; Yu, M.; Sun, X.; Woolley, A. T. Microdevices integrating affinity columns and capillary electrophoresis for multibiomarker analysis in human serum. *Lab Chip.* **2010,** *10*, 2527-33.

15. Ho, C. M. B.; Ng, S. H.; Li, K.H.; Yoon, Y.J. 3D printed microfluidics for biological applications. *Lab Chip.* **2015,** *15*, 3627-37.

16. Berman, B. 3-D printing: The new industrial revolution. *Bus. Horiz.* **2012,** *55* (2), 155-162.

17. Waheed, S.; Cabot, J. M.; Macdonald, N. P.; Lewis, T.; Guijt, R. M.; Paull, B.; Breadmore, M. C. 3D printed microfluidic devices: enablers and barriers. *Lab Chip.* **2016,** *16*, 1993-2013.

18. Gong, H.; Beauchamp, M.; Perry, S.; Woolley, A. T.; Nordin, G. P. Optical Approach to Resin Formulation for 3D Printed Microfluidics. *RSC Adv.* **2015,** *5*, 106621-106632.

19. Stansbury, J. W.; Idacavage, M. J. 3D printing with polymers: Challenges among expanding options and opportunities. *Dent. Mater.* **2016,** *32*, 54-64.

20. Gong, H.; Bickham, P, B.; Woolley, A, T.; Nordin, G. P. Custom 3D printer and resin for 18 μ m × 20 μ m microfluidic flow channels. *Lab Chip.* **2017,** *17,* 2899-2909

21. Gong, H.; Woolley, A. T.; Nordin, G. P. 3D printed high density, reversible, chip-to-chip microfluidic interconnects. *Lab Chip.* **2018,** *18*, 639-647.

22. Gong, H.; Woolley, A. T.; Nordin, G. P. High density 3D printed microfluidic valves, pumps, and multiplexers. *Lab Chip.* **2016,** *16*, 2450-2458.

23. Beauchamp, M. J.; Nielsen, A. V.; Gong, H.; Nordin, G. P.; Woolley, A. T. 3D Printed Microfluidic Devices for Microchip Electrophoresis of Preterm Birth Biomarkers. *Anal. Chem.* **2019,** *91*, 7418-7425.

24. Parker, E. K.; Nielsen, A. V.; Beauchamp, M. J.; Almughamsi, H. M.; Nielsen, J. B.; Sonker, M.; Gong, H.; Nordin, G. P.; Woolley, A. T. 3D printed microfluidic devices with immunoaffinity monoliths for extraction of preterm birth biomarkers. *Anal. Bioanal. Chem.* **2019,** *411*, 5405-5413.

25. Bickham, A. V.; Pang, C.; George, B. Q.; Topham, D. J.; Nielsen, J. B.; Nordin, G. P.; Woolley, A. T. 3D Printed Microfluidic Devices for Solid-Phase Extraction and On-Chip Fluorescent Labeling of Preterm Birth Risk Biomarkers. *Anal. Chem.* **2020,** *92*, 12322-12329.

26. Svec, F.; Lv, Y. Advances and recent trends in the field of monolithic columns for chromatography. *Anal. Chem.* **2015,** *87*, 250-73.

27. Knob, R.; Sahore, V.; Sonker, M.; Woolley, A. T. Advances in monoliths and related porous materials for microfluidics. *Biomicrofluidics.* **2016,** *10*, 032901.

28. Svec, F. Porous polymer monoliths: amazingly wide variety of techniques enabling their preparation. *J. Chromatogr. A.* **2010,** *1217*, 902-24.

29. Sonker, M.; Parker, E. K.; Nielsen, A. V.; Sahore, V.; Woolley, A. T. Electrokinetically operated microfluidic devices for integrated immunoaffinity monolith extraction and electrophoretic separation of preterm birth biomarkers. *Analyst.* **2017,** *143*, 224-231.

30. Jiang, T.; Mallik, R.; Hage, D.; S. Affinity Monoliths for Ultrafast Immunoextraction. *Anal. Chem.* **2005,** *77,* 2362-2372.

31. Knob, R.; Hanson, R. L.; Tateoka, O. B.; Wood, R. L.; Guerrero-Arguero, I.; Robison, R. A.; Pitt, W. G.; Woolley, A. T. Sequence-specific sepsis-related DNA capture and fluorescent labeling in monoliths prepared by single-step photopolymerization in microfluidic devices. *J Chromatogr. A.* **2018,** *1562*, 12-18.

32. Kang, Q. S.; Shen, X. F.; Hu, N. N.; Hu, M. J.; Liao, H.; Wang, H. Z.; He, Z. K.; Huang, W.; H. A 3D porous polymer monolith-based platform integrated in poly(dimethylsiloxane) microchips for immunoassay. *Analyst.* **2013,** *138*, 2613-9.

33. Reverte, L.; Prieto-Simon, B.; Campas, M. New advances in electrochemical biosensors for the detection of toxins: Nanomaterials, magnetic beads and microfluidics systems. A review. *Anal. Chim. Acta.* **2016,** *908*, 8-21.

34. Ng, E.; Chen, K.; Hang, A.; Syed, A.; Zhang, J. X. Multi-Dimensional Nanostructures for Microfluidic Screening of Biomarkers: From Molecular Separation to Cancer Cell Detection. *Ann. Biomed. Eng.* **2016,** *44*, 847-62.

35. Lipman, N, S.; Jackson, L, R.; Trudel, l. J.; Weis-Garcia, F. Monoclonal Versus Polyclonal Antibodies: Distinguishing Characteristics, Applications, and Information Resources. *ILAR. Journal.* **2005,** *46*.

36. Lenhard-Vidal, A.; Assolini, J. P.; Chiyoda, F. A. S.; Ono, M. A.; Sano, A.; Itano, E. N. Polyclonal antibodies to Paracoccidioides brasiliensisare able to recognise antigens from

different strains from Paracoccidioides species complex, including Paracoccidioides lutzii LDR2. *Mycoses.* **2018,** *61*, 826-832.

37. Laigre, E.; Goyard, D.; Tiertant, C.; Dejeu, J.; Renaudet, O. The study of multivalent carbohydrate-protein interactions by bio-layer interferometry. *Org. Biomol. Chem.* **2018,** *16*, 8899-8903.

38. Vala, M.; Jordan, L. R.; Warrington, A. E.; Maher, L. J., 3rd; Rodriguez, M.; Wittenberg, N. J.; Oh, S. H. Surface Plasmon Resonance Sensing on Naturally Derived Membranes: A Remyelination-Promoting Human Antibody Binds Myelin with Extraordinary Affinity. *Anal. Chem.* **2018,** *90*, 12567-12573.

39. Abdiche, Y.; Malashock, D.; Pinkerton, A.; Pons, J. Determining kinetics and affinities of protein interactions using a parallel real-time label-free biosensor, the Octet. *Anal. Biochem.* **2008,** *377*, 209-17.

40. Jahanshahi, P.; Wei, Q.; Jie, Z.; Ghomeishi, M.; Sekaran, S. D.; Mahamd Adikan, F. R. Kinetic analysis of IgM monoclonal antibodies for determination of dengue sample concentration using SPR technique. *Bioengineered.* **2017,** *8*, 239-247.

2. IMMUNOAFFINITY MONOLITHS FOR PEPTIDE EXTRACTION FROM BLOOD SERUM IN 3D PRINTED MICROFLUIDIC DEVICES

2.1 Introduction

Preterm birth (PTB) is birth that occurs prior to week 37 of pregnancy. It is the most common type of complication in pregnancy with an incidence rate of 1 out of every 9 births in the United States.[1-4] PTB is also a contributing cause in most neonatal deaths. Preterm infants can have multiple problems throughout their lives such as hearing and vision loss, acute respiratory failure, behavioral problems, sensory difficulty, and chronic lung disease.[5] No clinical methods are currently available to evaluate PTB risk at an early stage in pregnancy when intervention can still delay delivery. Thus, there is a major need for an inexpensive and rapid diagnostic method that can accurately evaluate the risk of PTB. Recently, nine maternal serum PTB biomarkers were identified that show significant predictive power for the onset of early labor.[3]

Due to their micro-scale dimensions (<100 μm), microfluidic devices offer multiple advantages over conventional laboratory instrumentation. Microfluidic devices use lower volumes of sample and reagents, making them ideal for handling costly or toxic chemicals.[6] Moreover, the small size of microfluidic devices results in faster analysis times, better temperature control, lower energy consumption, and portability.[7] All these benefits make microfluidic devices a promising platform for sensitive and cheap analysis. Originally, microfluidic devices were fabricated using photolithography in silicon or glass. This method requires multiple costly and complicated processes, including patterning, bonding, and etching steps,[8-9] so alternative techniques to overcome these limitations are needed.[10]

Polydimethylsiloxane (PDMS) and thermoplastics are commonly used materials to create microfluidic devices. PDMS is easy to mold and prototype, biocompatible, and optically clear. These features make it an attractive material for use in many different experiments.[11- 12] However, PDMS is easily torn during fabrication and is prone to nonspecific adsorption.[13] Thermoplastics are another useful fabrication material because they can be optically clear, inexpensive, and easily batch fabricated.[14] However, many have poor resistance to non-polar solvents, and it can be challenging to bond multiple layers during the fabrication process.[15-16]

3D printing is an additive manufacturing process that creates 3D objects layer by layer from a computer designed file.[17] These features make this technology useful in many applications like dentistry and the aerospace industry to create precise models, prototypes, and patterns.[18] 3D printing has numerous advantages over traditional microfabrication techniques, such as offering lower setup costs, not requiring a cleanroom environment, and using fewer toxic chemicals.[19, 20] Recently, 3D-printed microdevices have received attention due to the potential for rapid, iterative optimization, where experimental data can provide feedback to improve design.[21] One type of 3D printing called stereolithography (SL) uses a liquid resin that is photopolymerized one layer at a time through exposure to UV light. A customized SL 3D printer built by Nordin's group at BYU has been used to make 20 μm × 20 μm channels in complex fluidic patterns.[22]

A monolith is a porous polymer, and these materials have been researched for more than two decades, resulting in the development of many applications.[23] Monoliths can have a high flow rate, enhanced mass transfer resistance, and low backpressure compared to traditional packed bead columns.[24] Immunoaffinity monoliths have been used to retain target analyte in a column. Kang et al.[25] used affinity monoliths to carry out microfluidic immunoassays for H1N1

influenza virus. Furthermore, Parker et al.[26] used an affinity monolith to extract ferritin, a PTB biomarker, from human blood serum.

Here I have further developed immunoaffinity columns to extract CRF, a peptide PTB biomarker, in a 3D printed device. I 3D printed 45 μm × 50 μm enclosed microfluidic channels for immunoaffinity extraction. I used vacuum driven flow to extract CRF on an anti-CRF monolith column. First, I demonstrated the binding between CRF and anti-CRF using a dot blot. Next, I fluorescently labeled the anti-CRF and verified its attachment to the monolith using CCD images. Lastly, I used an anti-CRF monolith column to extract CRF from both buffer and spiked blood serum. My data show successful retention and elution of CRF from anti-CRF column. This is the first demonstration of extracting a PTB peptide from human blood serum using a 3D-printed microfluidic device. This study further shows the strong promise for using these immunoaffinity columns to extract all nine PTB biomarkers from blood serum as part of a PTB diagnostic system.

2.2 MATERIALS AND METHODS

2.2.1 Chemicals

Anti-corticotropin releasing factor (anti-CRF, produced in rabbit), glycidyl methacrylate (GMA), ethylene glycol dimethacrylate (EDMA), 1- dodecanol, 2,2-dimethoxy-2-phenylacetophenone (DMPA), poly (ethylene glycol) diacrylate (PEGDA, MW 250), Tris hydrochloride, 3-(trimethoxysilyl) propyl methacrylate, dimethyl sulfoxide (DMSO), and phenylbis (2,4,6 trimethylbenzoyl) phosphine oxide (Irgacure 819) were purchased from Sigma (St. Louis, MO). Amicon ultra 0.5-mL centrifugal filters (3, and10 kDa cutoff), boric acid, sodium phosphate, sodium bicarbonate, and sodium carbonate were obtained from Millipore Sigma (Burlington, MA). Solutions were made using deionized water (18.3 MΩ) filtered by a

Barnstead EASY- pure UV/ UF system (Dubuque, IA). Alexa Fluor 532 (carboxylic acid, succinimidyl ester) and Tris base were purchased from Fisher Scientific (Fair Lawn, NJ). Isopropyl alcohol (IPA) was from Macron (Center Valley, PA). Sodium hydroxide was obtained from Mallinckrodt Baker (Paris, KY). Glass slides for 3D printing were purchased from VWR (Radnor, PA). Cyclohexanol was obtained from Spectrum (New Brunswick, NJ). 2-Nitrophenyl phenyl sulfide (NPS) came from TCI (Portland, OR). Dry milk was purchased from Walmart (Bentonville, AR). Nitrocellulose paper was obtained from Bio-Rad (Hercules, CA), and labeled secondary antibody (IRDye 800CW goat anti-rabbit IgG came from LICOR (Lincoln, NE). CRF came from GeneScript (Piscataway, NJ), and PTB peptide 2 (P2) was purchased from Biomatik (Wilmington, DE). Female human blood serum (off-the-clot, sterile filtered) was purchased from Zen-Bio (Research Triangle Park, NC).

2.2.2 3D Printed Microfluidic Devices

I used a custom 3D printer[22] to create the design shown in Figure 2.1A-B. The design has five separated channels, each 5 layers high and 6 pixels wide (50 μm x 45 μm), with a reservoir on one end and a port in the other end to connect to vacuum. Devices also have a window for polymerization of the monolith that is 600 μm wide and 6 layers above the channel.[26] The material used for fabricating 3D printed devices is 97% PEGDA, 2% NPS UV absorber, and 1% Irgacure 819 photoinitiator.

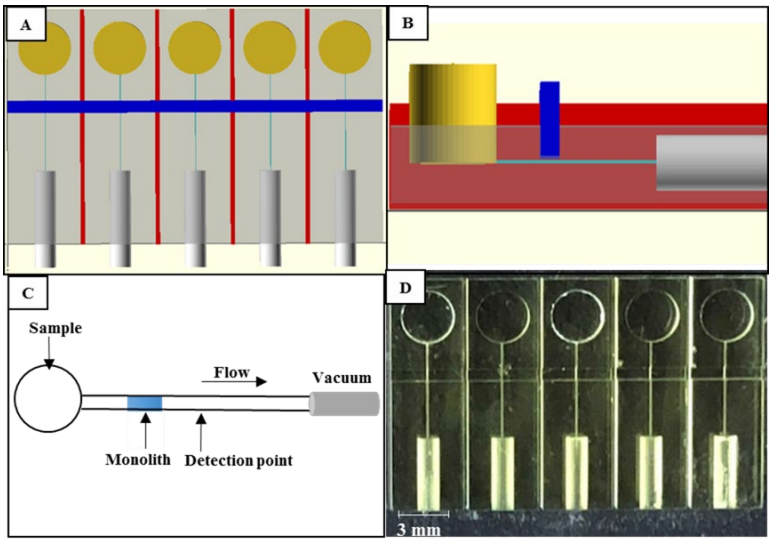

Figure 2.1 3D printed devices for affinity extraction. (A) OpenSCAD design. Reservoirs are yellow, channels are green, the monolith polymerization window is blue, and the device divisions are red (B) Cross section of device design. (C) Diagram of device operation for peptide extraction. The labeled peptide is flowed through the channel by applying vacuum; as labeled analyte passes the detection point, the signal is recorded. (D) Photograph of 3D printed device.

2.2.3 Sample Preparation

CRF and peptide 2 were fluorescently labeled by dissolving in 10 mM bicarbonate buffer (BCB, pH 10). Alexa Fluor 532 was dissolved in DMSO and added to each biomarker. CRF (200 µM) and peptide 2 (40 µM) were labeled in 10 mM BCB pH 10 at a dye:biomarker molar ratio of 3:2 at room temperature overnight. Next, peptide 2 was filtered four times at 14,000 RPM for 15 min using an Amicon 3-kDa cutoff filter to remove excess dye. Then, samples were diluted to the desired concentration in 20 mM phosphate buffer at pH 7. The anti-CRF was labeled at a dye:antibody molar ratio of 10:1, and sample was filtered four times at 14,000 RPM for 15 min using an Amicon 10-kDa cutoff filter to remove excess dye. The spiked CRF sample was prepared by adding labeled CRF to yield a 300 nM concentration in human blood serum, which was five-fold diluted in 20 mM phosphate buffer, pH 7.

2.2.4 Monolith Formation

Monoliths were prepared as described by Parker et al.[26] using 24% GMA, 11% EDMA, 10% cyclohexanol and 55% 1-dodecanol. The solution was sonicated for 10 min, 1% DMPA photoinitiator was added, and the mixture was sonicated for an additional 10 minutes. Then, the mixture was allowed to fill the channels by capillary action, and the entire device was exposed to UV light (SunRay 600, Uvitron, West Springfield, MA) for 10 min, which polymerized the monolith at the desired location in the channel through the polymerization window built into the design. The unpolymerized mixture was removed from the monolith by flushing the channels with IPA for 30 min using vacuum.

2.2.5 Antibody characterization and immobilization

A dot blot experiment was performed to test the compatibility of anti-CRF toward CRF. First, 2 μL of CRF (1 mg/mL) was dotted on nitrocellulose paper. After drying the dot for 30 min, a blocking step was performed using 5% milk in 10× Tris buffer saline (TBS) for 1 h to block the rest of the paper. Next, the paper was submerged in antibody solution (1 μg/mL in TBS plus 0.05 % Tween 20; TBST) and incubated for 1 h on a rotator. Then, the paper was washed thoroughly using TBST for 15 min, and the secondary antibody (1 μg/mL in TBS) for fluorescence detection was added and incubated for 1 h. Next, the paper was washed again with TBST for 15 min. Finally, scans of dot blots were taken using a LI-COR ODYSSEY imaging system.

To attach antibody to the monolith, 4 μL of solution (9.5 mg/mL) was added to the device reservoir and allowed to flow through the monolith by capillary action. Then, the reservoirs were filled with 20 mM borate buffer (pH 8) and sealed to prevent evaporation. Devices were incubated for 7 h at room temperature in a humid chamber to provide sufficient

time for primary amines on the antibody to react with epoxy groups on the GMA monolith. Next, the remaining epoxy groups in the monolith were blocked by flowing 0.1 M Tris buffer (pH 8.5) through for 1 h. After blocking, the monoliths were thoroughly washed with 20 mM phosphate buffer (pH 7). For control experiments no antibody was added, but the monolith was blocked using Tris buffer. I applied vacuum as shown in Figure 2.1C to move analytes in 3D printed devices.

The attachment of anti-CRF to a GMA monolith was verified using CCD fluorescence images. I directed a 532 nm laser through a 4X objective and took CCD images with 300 ms exposure times. First, an image of the monolith was taken before attaching the antibody. Then, anti-CRF labeled with Alexa Fluor 532 was immobilized onto the monolith overnight. Then, the monolith was rinsed with 20 mM borate buffer pH 8 for 30 min and another image was taken of the monolith. Image J was used to measure the background-subtracted fluorescence of the monolith with labeled antibody compared to the control.

2.2.6 Experimental Setup

Experimental conditions followed those found in a published paper.[26] I used a 532 nm laser to induce fluorescence. The signal was recorded with a photomultiplier tube and digitized using LabVIEW software. Experiments were conducted as follows. First, channels were filled with 20 mM phosphate buffer pH 7, and vacuum was applied for 1 min through the device port to equilibrate as seen in Figure 2.1C. Then, vacuum was removed, the reservoir was emptied and fluorescently labeled sample was loaded into the reservoir and channel by applying vacuum for one additional minute. The labeled sample was incubated on the monolith for 10 min, the reservoir was washed three times with phosphate buffer, and the monolith was rinsed using 20 mM phosphate buffer (pH 7) for 6 min for sample loaded in buffer and 8 min for blood serum.

Finally, reservoirs were filled with 50 mM bicarbonate buffer (pH 10) and vacuum was applied for 1 min to elute the sample.

2.3 RESULTS AND DISCUSSION

2.3.1 Dot Blot Tests

I used a dot blot to confirm the compatibility of CRF toward anti-CRF, as seen in Figure 2.2. Figure 2.2A shows two fluorescence dots for a positive control of ferritin and anti-ferritin, demonstrating the binding between the ferritin and anti-ferritin. Figure 2.2B shows two similar bright fluorescent dots, indicative of strong binding of CRF to anti-CRF. These dot blots show that the anti-CRF antibody chosen is suitable for CRF.

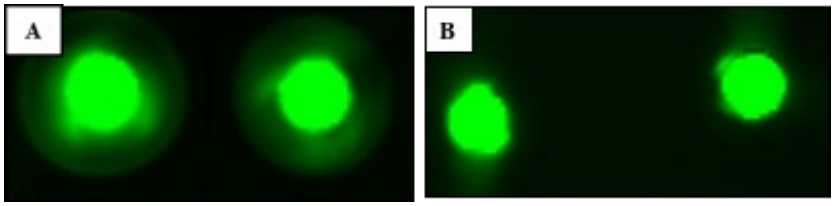

Figure 2.2 Dot blot assay on nitrocellulose membrane. Two duplicate dots of (A) positive control with ferritin and anti-ferritin; and (B) CRF and anti-CRF.

2.3.2 Immunoaffinity Monoliths in 3D Printed Devices

The 3D printed devices are seen in Figure 2.1D. My devices match the design files in Figure 2.1A-B with five independent channels. I successfully formed monoliths inside my 3D printed devices as seen in Figure 2.3A. The morphology of the GMA monoliths was determined using scanning electron microscopy (SEM) as seen in Figure 2.3B-C. Monolith pore and nodule sizes were analyzed using ImageJ, and were 1.5 ± 0.6 μm (n=50) and 0.49 ± 0.08 μm (n=50), respectively. The SEMs images show that my monoliths were well polymerized and anchored to the microfluidic channel wall. This wall attachment is essential for good flow and analyte interaction with the monolith.

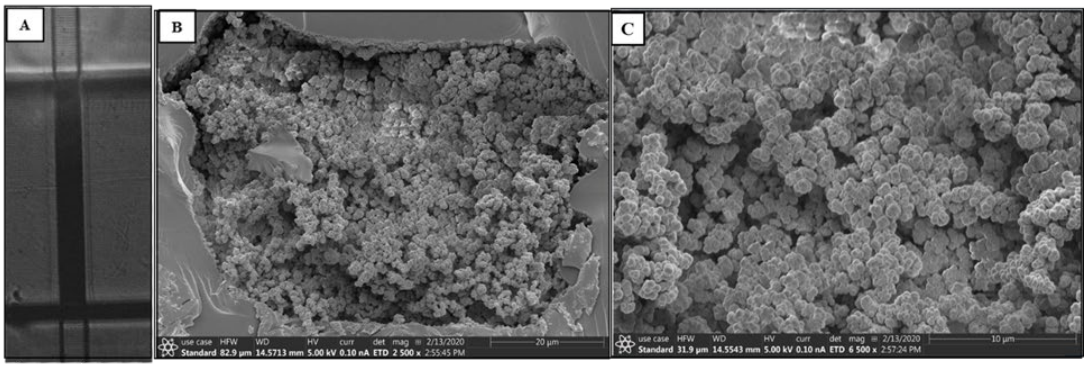

Figure 2.3 Formation of a monolith in a 3D printed microfluidic device. (A) Photograph of monolith inside a channel. (B-C) SEM images of monoliths prepared from GMA with 10-min exposure in a 3D printed microfluidic device; (B) channel view and (C) zoom view.

To verify the attachment of anti-CRF to a GMA monolith, I used fluorescence imaging. A fluorescence image of a monolith before attaching the antibody is shown in Figure 2.4A. A monolith after attachment of AlexaFluor 532 labeled anti-CRF and rinsing is seen in Figure 2.4B. The fluorescence on the control monolith in Figure 2.4A is much dimmer compared to the monolith that had the fluorescently labeled anti-CRF attached. These images show differences between the control monolith and the antibody-modified monolith, clearly indicating that anti-CRF was successfully attached to the GMA monolith. Figure 2.4C shows the background-subtracted fluorescence measurement for the monolith with labeled antibody compared to the control. The fluorescence signal was significantly increased compared to the blank, confirming that anti-CRF was attached to the monolith.

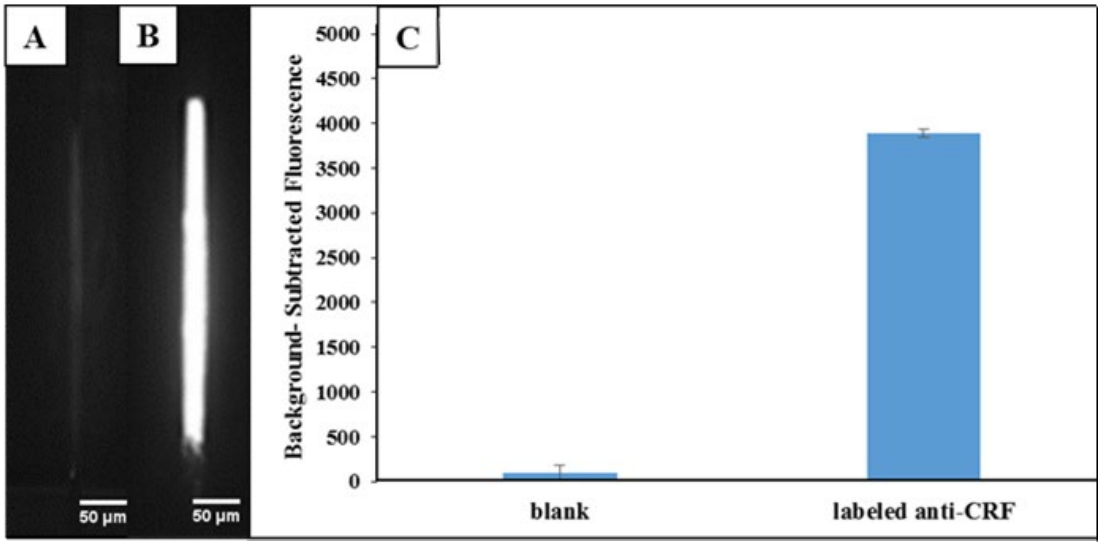

Figure 2.4 Labeled antibody attachment. Fluorescence images of (A) control and (B) labeled anti-CRF fluorescence monoliths. (C) Background-subtracted fluorescence of the monolith before and after immobilization of labeled anti-CRF.

2.3.3 Immunoaffinity Extraction of CRF Using 3D Printed Microfluidic Devices

I studied CRF retention and elution when there was no antibody on the monolith, and when anti-CRF was immobilized on the monolith as seen in Figure 2.5. In both experiments, labeled CRF in either buffer or blood serum was loaded into the channel, which caused an increase in the fluorescent signal on the monolith. After rinsing nonspecifically bound labeled analyte from the monolith, the fluorescent signal on the monolith drops. Upon eluting, fluorescence on the monolith further decreases, confirming that retained CRF on the anti-CRF monolith was removed.

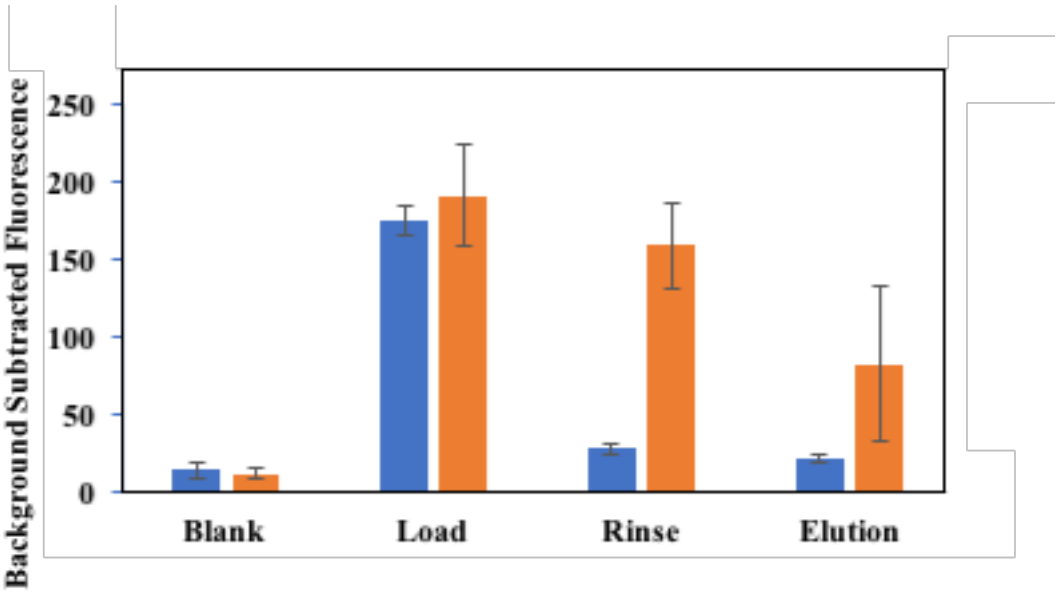

Figure 2.5 Fluorescence signal from the monolith during the extraction of CRF from human blood serum diluted five-folds and spiked with 300 nM CRF. (Blue) control monolith (no anti-CRF); (orange) monolith with (anti-CRF).

Point detection of fluorescence after the monolith during elution (see Figure 2.1C) showed a peak at 10 seconds for the anti-CRF column, compared to no peak observed from the blocked monolith, as seen in Figure 2.6A. These results demonstrate successful elution of retained CRF loaded from buffer using an anti-CRF monolith. I completed a similar experiment using blood serum diluted 1:5 in buffer and spiked with CRF as seen in Figure 2.6B. A small increase in fluorescence at five seconds was seen for both the anti-CRF and blocked columns. This feature may arise from elution of nonspecifically adsorbed components present in the blood serum. A much larger increase observed at 10 second was only seen for elution from the anti-CRF monolith. This demonstrates elution of CRF selectively retained from spiked blood serum in the anti-CRF column.

I also tested the selectivity of anti-CRF toward a different PTB peptide biomarker by loading labeled peptide 2 on an anti-CRF column and eluting. As seen in Figure 2.6C

fluorescence during elution showed narrow, small peaks at five seconds for both anti-CRF and blocked columns. These peaks likely resulted from a minor amount of nonspecific adsorption of peptide 2 to the monolith. These data confirm that the binding between CRF and anti-CRF relative to the peptide 2 PTB biomarker in a 3D-printed device is selective.

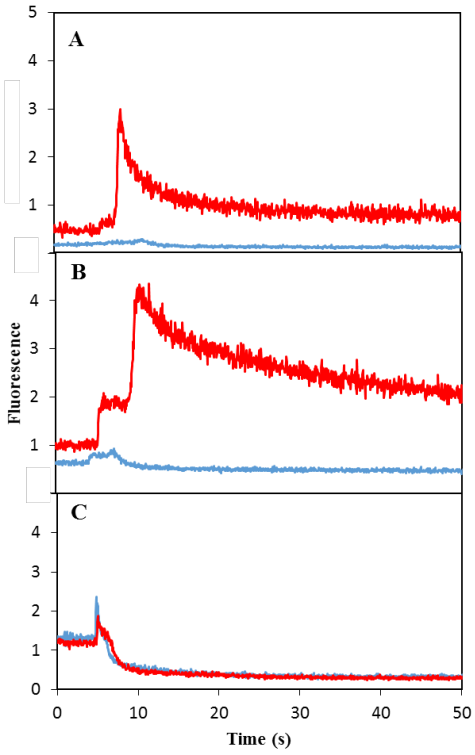

Figure 2.6 Fluorescence elution profile on an anti-CRF monolith (red) or a control monolith lacking attached antibody (blue) of (A-B) 300 nM AF532-labeled CRF from (A) buffer and (B) human blood serum (diluted 5-fold), or (C) 150 nM AF532-labeled peptide 2.

I used a custom 3D printer to create microfluidic devices with immunoaffinity monoliths for selective retention and elution of CRF from human blood serum. These 3D-printed devices are easy to prototype and can make 3D microfluidic features. This is the first demonstration of an immunoaffinity column in a 3D-printed device for extraction of a peptide biomarker from both buffer and blood serum. This study is an important step towards the goal of multiplexed analysis of PTB biomarkers from serum in a single 3D printed microfluidic device.

2.4 REFERENCES

1. Blencowe, H.; Cousens, S.; Chou, D.; Oestergaard, M.; Say, L.; Moller, A. B.; Kinney, M.; Lawn, J. Born Too Soon: The global epidemiology of 15 million preterm births, *Reprod. Health.* **2013,** *10*, S2.

2. Rush, R. W. K.; M., Howat, P.; Baum, J. D.; Anderson, A. B. M.; Turnbull, A. C. Contribution of preterm delivery to prinatal mortality. *Br. Med.J.* **1976,** *2*, 965-968.

3. Esplin, M. S.; Merrell, K.; Goldenberg, R.; Lai, Y., Iams; J. D.; Mercer, B.; Spong, C. Y.; Miodovnik, M.; Simhan, H. N.; van Dorsten, P.; Dombrowski, M. Proteomics Identification of Serum Peptides Predicting Subsequent Spontaneous Preterm Birth. *Am. J. Obstet. Gynecol.* **2011,** *204*, 391 e1-8.

4. Centers for Disease Control and Prevention. Reproductive Heath: Preterm Birth. http://www.cdc.gov/reproductivehealth/maternalinfanthealth/pretermbirth.htm. (accessed 21 October **2019**).

5. Behrman, R. E. B.; A. S. "Preterm Birth: Causes, Consequences, and Prevention," National Academies Press (US): Washington DC, **2007**.

6. Whitesides, G. M., The origins and the future of microfluidics, *Nature* **2006,** *442*, 368-373.

7. Pandey, C. M.; Augustine, S.; Kumar, S.; Kumar, S.; Nara, S.; Srivastava, S.; Malhotra, B. D. Microfluidics Based Point-of-Care Diagnostics. *J. Biotechnol.* **2018,** *13*, 1700047.

8. Qi, Z.; Xu, L.; Xu, Y.; Zhong, J.; Abedini, A.; Cheng, X.; Sinton, D. Disposable silicon-glass microfluidic devices: precise,robust and cheap. *Lab Chip.* **2018,** *18*, 3872-3880.

9. Nge, P. N.; Rogers, C. I.; Woolley, A. T. Advances in Microfluidic Materials, Functions, Integration, and Applications. *Chem. Rev.* **2013,** *113*, 2550-2583.

10. Ho, C. M., Ng, S. H., Li, K. H., Yoon, Y. J., 3D printed microfluidics for biological applications. *Lab Chip.* **2015,** *15*, 3627-3637.

11. Nielsen, J. B.; Hanson, R. L.; Almughamsi, H. M.; Pang, C.; Fish, T. R.; Woolley, A. T. Microfluidics: Innovations in Materials and Their Fabrication and Functionalization. *Anal. Chem.* **2020,** *92*, 150-168.

12. Lee, S.; Kim, H.; Lee, W.; Kim, J. Finger-triggered portable PDMS suction cup for equipment-free microfluidic pumping. *Micro Nano Syst. Lett.* **2018,** *6*, 1-5

13. Toepke, M. W.; Beebe, D. J. PDMS absorption of small molecules and consequences in microfluidic applications. *Lab Chip.* **2006,** *6*, 1484-1486.

14. Liu, K.; Fan, Z. H. Thermoplastic microfluidic devices and their applications in protein and DNA analysis. *Analyst.* **2011,** *136*, 1288-1297.

15. Tsao, C.-W.; DeVoe, D. L. Bonding of thermoplastic polymer microfluidics, *Microfluid. Nanofluidics.* **2009,** *6*, 1-16.

16. Gencturk, E.; Mutlu, S.; Ulgen, K. O. Advances in microfluidic devices made from thermoplastic used in cell biology and analyses. *Biomicrofluidics.* **2017,** *11*, 051502.

17. Berman, B. 3-D printing: The new industrial revolution, *Bus. Horiz.* **2012,** *55*, 155-162.

18. Stansbury, J. W.; Idacavage, M. J. 3D printing with polymers: Challenges among expanding options and opportunities. *Dent. Mater.* **2016,** *32*, 54-64.

19. Waheed, S.; Cabot, J. M.; Macdonald, N. P.; Lewis, T.; Guijt, R. M.; Paull, B.; Breadmore, M. C. 3D printed microfluidic devices: enablers and barriers. *Lab Chip.* **2016,** *16*, 1993-2013.

20. Gong, H. B.; M., Perry, S.; Woolley, A. T.; Nordin, G. P. Optical Approach to Resin Formulation for 3D printed Microfluidics. *RSC Adv.* **2015,** *5*, 106621-106632.

21. Beauchamp, M. J.; Nordin, G. P.; Woolley, A. T. Moving from millifluidic to truly microfluidic sub-100-μm cross-section 3D printed devices. *Anal. Bioanal. Chem.* **2017,** *409*, 4311-4319.

22. Gong, H.; Bickham, B. P.; Woolley, A. T.; Nordin, G. P. Custom 3D printer and resin for 18 μm × 20 μm microfluidic flow channels. *Lab Chip.* **2017,** *17*, 2899-2909.

23. Svec, F.; Lv, Y. Advances and Recent Trends in the Field of Monolithic columns for Chromatography. *Anal. Chem.* **2015,** *87*, 250-273.

24. Andjelkovic, U.; Tufegdzic, S.; Popovic, M. Use of monolithic supports for high-throughput protein and peptide separation in proteomics. *Electrophoresis.* **2017,** *38*, 2851-2869.

25. Kang, Q. S.; Shen, X. F.; Hu, N. N.; Hu, M. J.; Liao, H.; Wang, H. Z.; He, Z. K.; Huang, W. H. A 3D porous polymer monolith-based platform integrated in poly(dimethylsiloxane) microchips for immunoassay. *Analyst*. **2013,** *138*, 2613-2619.

26. Parker, E. K.; Nielsen, A. V.; Beauchamp, M. J.; Almughamsi, H. M.; Nielsen, J. B.; Sonker, M.; Gong, H.; Nordin, G. P.; Woolley, A. T. 3D printed microfluidic devices with immunoaffinity monoliths for extraction of preterm birth biomarkers. *Anal. Bioanal.Chem.* **2019,** *411*, 5405-5413.

3. CHARCTERIZATION OF ANTIBODIES TARGETING PTB BIOMARKERS FOR IMMUNOAFFINITY EXTRACTION

3.1 Introduction

Finding a compatible antibody to target an antigen is essential in immunoaffinity assays. The binding between antigen and antibody is influenced by non-covalent intermolecular interactions such as hydrogen bonding, electrostatic interactions, hydrophobic interactions, and Van der Waals forces between the two molecules.[1]

Antibodies are produced from B cells and can be either polyclonal or monoclonal.[2-3] Polyclonal antibodies have the affinity to recognize their target antigen as well as similar epitopes if the epitope has a sequence match to the antibody. However, monoclonal antibodies are highly specific and only recognize a specific epitope. Identifying specific antibodies for PTB biomarkers facilitates immunoaffinity extraction. Cross reactivity can occur when the antibody has affinity to bind to multiple antigens. This phenomenon is often observed in polyclonal antibodies that contain a heterogeneous mixture of antibodies produced from different B cells.[4]

Dot blotting is a rapid technique that is widely used to examine compatibility between antigen and antibody. Antigen-antibody interactions are more precisely measured by traditional techniques such as ELISA,[5-7] radioimmunoassay,[8] or isothermal titration calorimetry.[9] Although these techniques are effective, they are also time consuming, require labeled samples, and are expensive.[10] However, alternative methods are now available to study the interaction between molecules,[11] which are label free, high throughput, and fast.[12-13] Two common biosensor techniques are BLI and SPR.[12-15] Both are widely used, generate quick results, and provide quantitative data to study the intermolecular interaction between antigen-antibody complexes.

Understanding the mathematical basis of the interaction between the antigen-antibody complex is significant for the quality of an immunoassay. The equilibrium between the antibody (Ab) and antigen (Ag) is reversible, and generates the antibody-antigen complex (Ab-Ag), which is expressed via equation (3.1).[2]

$$[Ab]+[Ag] \rightleftharpoons [Ab\text{-}Ag] \quad (3.1)$$

The association and dissociation constants are represented by K_a and K_d, respectively. [Ab] is the antibody concentration, [Ag] is the antigen concentration, and [Ab-Ag] is the concentration of complex in the bound state. K_a and K_d are calculated as shown in equations (3.2) and (3.3).

$$K_a = k_{on} / k_{off} = [Ab\text{-}Ag] / [Ab][Ag] \quad (3.2)$$

$$K_d = k_{off} / k_{on} = [Ab][Ag] / [Ab\text{-}Ag] \quad (3.3)$$

The closer K_d is to zero, the tighter the binding in the Ab-Ag complex and the more stable the interaction between the complex will be. The value of K_d corresponds to the concentration of the ligand at which half of the antigen is saturated at equilibrium. Knowing K_d values helps to determine which analyte will dissociate more readily from a multiplex antibody column, based on which has the strongest or weakest interaction with its target. This information is needed for extraction of all nine PTB biomarkers from human blood serum.

Determination of the strength of binding between PTB biomarkers and their targeted antibodies is a significant step in the development of multiplex immunoaffinity columns. In this chapter, I present the data for either monoclonal or polyclonal antibody characterization, cross reactivity for multiple PTB biomarkers, and outcomes of immunoaffinity extraction. BLI of several PTB biomarkers, ferritin, lactoferrin, and CRF, toward their polyclonal antibodies is also reported.

3.2 MATERIALS AND METHODS

3.2.1 Reagents

Ferritin was obtained from EMD Millipore (Billerica, MA). Lactoferrin, anti-lactoferrin (produced in rabbit), anti-ferritin (produced in rabbit), and anti-corticotropin releasing factor (anti-CRF, produced in rabbit) were purchased from Sigma (St. Louis, MO). CRF came from GenScript (Piscataway, NJ). PTB, peptide 2, and peptide 3, and biotinylated CRF were purchased from Biomatik (Wilmington, DE). Sodium phosphate was obtained from Millipore Sigma (Burlington, MA). Alexa Fluor 532 (carboxylic acid, succinimidyl ester) and Tris base were purchased from Fisher Scientific (Fair Lawn, NJ). EZ-Link Sulfo-NHS-LC-Biotin, monoclonal anti-CRF (produced in mice), and both polyclonal and monoclonal anti-ITIH4 were obtained from ThermoFisher (St. Louis, MO). Dry milk was purchased from Walmart (Bentonville, AR). Nitrocellulose paper was obtained from Bio-Rad (Hercules, CA), and IRDye 800CW labeled secondary goat anti-mouse IgG came from LICOR (Lincoln, NE). Streptavidin biosensors were purchased from ForteBio (Fermont, CA) and bovine serum albumin (BSA) was purchased from EMD Millipore. Assay workflow details are described in Chapter 4.1.7.

3.2.2 PTB Biomarker Preparation for Immunoaffinity Extraction

The PTB biomarkers were all fluorescently labeled and included ferritin, lactoferrin, TNF, peptide 2 and CRF dissolved in 10 mM bicarbonate buffer (BCB, pH 10). TAT was prepared as in Nielsen et al.[16] Alexa Fluor 532 was dissolved in DMSO, added to each biomarker, and incubated at room temperature overnight. Peptide 2 was heated at 37°C during labeling. All PTB biomarkers were labeled at the different dye:biomarker molar ratios shown in Table 3.1. Next, protein biomarkers were filtered four times at 14,000 RPM for 15 min using a

cutoff filter depending on their size. Samples were diluted to the desired concentration in 20 mM phosphate buffer pH 7 for ferritin, lactoferrin, TNF, and CRF, or at pH 8 for peptide 2. Peptide 2 was also spiked into human blood serum to a 500 nM concentration.

Table 3.1 Dye: PTB biomarker molar labeling ratio**.**

PTB Biomarker	Dye: Biomarker
Ferritin	30: 1
Lactoferrin	15: 1
TNF	20: 1
Peptide 2	40: 1
CRF	3: 2

3.2.3 Antibody Characterization and Immobilization

A dot blot experiment was performed to test the compatibility of either polyclonal or monoclonal antibodies toward PTB biomarkers as described in Chapter 2.5.

3.2.4 Immunoaffinity Experimental Setup

Experimental conditions are described in Chapter 2.6. Briefly, I used a 532 nm laser to induce fluorescence. First, channels were filled with either 20 mM phosphate buffer pH 7 or pH 8, and vacuum was applied through the device to move the PTB analyte. The labeled sample was incubated on the monolith for 10 min, followed by three washes with phosphate buffer. Finally, reservoirs were filled with 50 mM bicarbonate buffer (pH 10) and vacuum was applied for 1 min to elute the sample.

3.2.5 Kinetic Characterization

Ferritin and lactoferrin were dissolved in PBS pH 7 (at the concentration of 1 mg/mL) and then biotinylated as described in the ThermoFisher protocol for product No. A39257. CRF was synthesized with a biotin label at one end and then dissolved in PBS pH 7 at 1 mg/mL. All

biomarkers (CRF, ferritin, and lactoferrin) were loaded on the biosensor at 5-10 µg/mL. The association step was performed for 400 s for anti-CRF, 300 s for anti-ferritin, and 60 s for anti-lactoferrin for the different concentrations. The dissociation step was performed in the assay buffer for 800 s for CRF, 300 s for anti-ferritin, and 800 s for anti-lactoferrin in PBS pH 7. The BLI data for association and dissociation were analyzed by Octet Data Analysis 8.2 software and fit to a 1:1 binding model to obtain kinetic parameters.

3.3 Results and Discussion

3.3.1 Characterization of Polyclonal Antibodies Targeting PTB Biomarkers

Dot blots were used to evaluate binding of specific polyclonal antibodies to target PTB peptide biomarkers. Dot blots of polyclonal antibodies against ITIH4 (to target peptides 2 and 3) are shown in Figure 3.1, in addition to fluorescence dots for the lactoferrin and anti-lactoferrin positive control. These dot blots clearly show that the polyclonal antibodies selected are suitable for the PTB peptide biomarkers of peptide 2 and peptide 3.

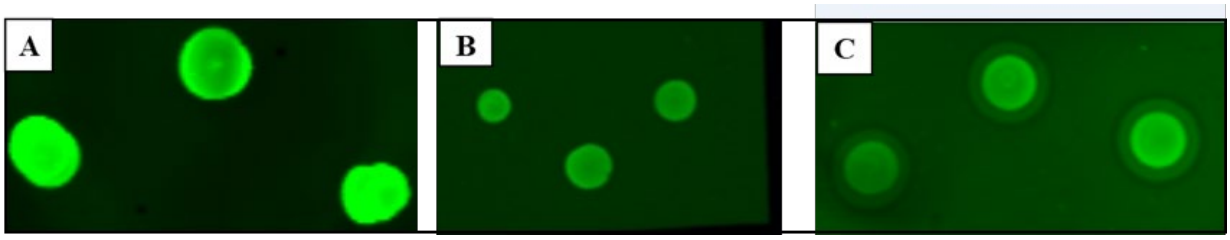

Figure 3.1 Dot blot assays on nitrocellulose membranes for polyclonal antibodies. Fluorescent dots of (A) positive control with lactoferrin and anti-lactoferrin, (B) peptide 2 and anti-ITIH4, and (C) peptide 3 and anti-ITIH4.

To extract multiple PTB biomarkers, I first developed individual immunoaffinity columns in a 3D printed microfluidic device for the extraction of two PTB biomarkers: CRF, and lactoferrin. Extraction of CRF using polyclonal anti-CRF is discussed in chapter 2. Elution of lactoferrin from its polyclonal antibody is seen in Figure 3.2, which shows an elution peak at 20

seconds from lactoferrin on an anti-lactoferrin column compared to a much smaller peak for the blocked column. This peak on the control column is a result of adsorption of lactoferrin. These data show successful retention and elution of another PTB protein biomarker, which combined with CRF extracted in Chapter 2, and ferritin extracted by Parker et al.,[17] is a further step toward extraction of all nine PTB biomarkers.

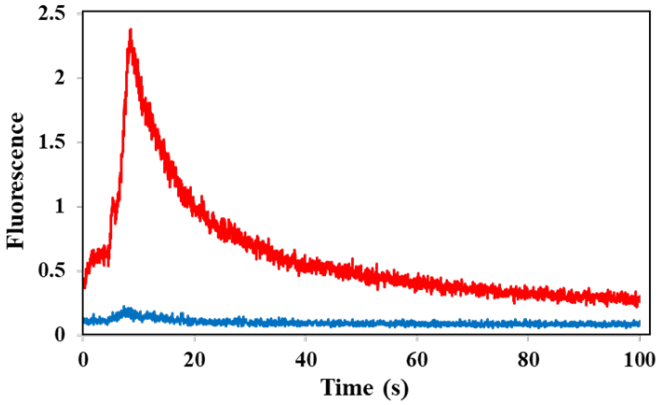

Figure 3.2 Fluorescence during elution after extraction of 50 nM AF532-labeled lactoferrin in 20 mM phosphate buffer pH 7 from a polyclonal antibody-modified column (red) or a control monolith lacking attached antibody (blue).

3.3.2 Selectivity of PTB Biomarker Extraction in Immunoaffinity Columns

To achieve successful capture of all nine PTB biomarkers using their respective polyclonal antibodies, I conducted an experiment to check whether there is cross reactivity between any of PTB biomarkers and off-target polyclonal antibodies using dot blots. Figure 3.3A shows fluorescent dots for ferritin and anti-ferritin as a positive control. Figure 3.3B shows fluorescent dots for ferritin on a non-target polyclonal antibody, anti-CRF, which indicates some cross reactivity between ferritin and anti-CRF polyclonal antibody. Figure 3.3C represents fluorescent dots for lactoferrin and anti-CRF, which indicates more cross reactivity. This high cross reactivity possibly resulted from adsorption of lactoferrin to the primary antibody. Figure 3.3D shows no fluorescence, which means no off-target binding was observed between CRF and polyclonal anti-ferritin. This could be due to the small size of the peptide that makes it hard to

recognize and bind to a non-target antibody. These data show off-target binding between PTB protein biomarkers, ferritin and lactoferrin, with polyclonal anti-CRF.

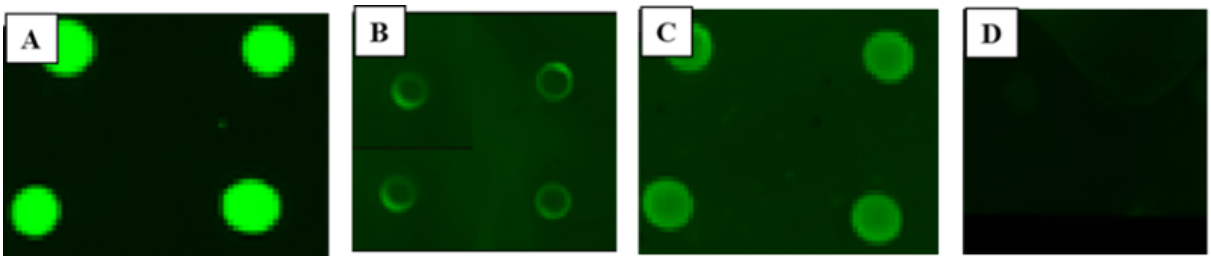

Figure 3.3 Dot blot assays on nitrocellulose membranes for polyclonal antibodies. Four duplicate dots of (A) positive control with ferritin and anti-ferritin. (B) ferritin and anti-CRF. (C) lactoferrin and anti-CRF. (D) CRF and anti-ferritin**.**

Another experiment was conducted to confirm the cross reactivity that was observed from polyclonal antibodies in dot blots. Fluorescently labeled ferritin was loaded on anti-lactoferrin column. Figure 3.4A shows an elution peak at 50 seconds for ferritin on the anti-lactoferrin column. However, when CRF was loaded on non-target polyclonal antibody column, no elution peak was detected, as seen in Figure 3.4B. This data shows no off-target binding observed between CRF and polyclonal anti-ferritin. To conclude, off-target interaction between PTB protein biomarkers and polyclonal antibodies occurs, but limited interaction is seen between PTB peptide biomarkers and non-target polyclonal antibodies. Although polyclonal antibodies have the ability to capture their target antigens effectively, I observed cross reactivity between PTB protein biomarkers and off-target antibodies. This is likely due to their ability to recognize multiple epitopes on different antigens. The cross reactivity between polyclonal antibodies and non-target analytes hindered the development of multiplex immunoaffinity extraction.

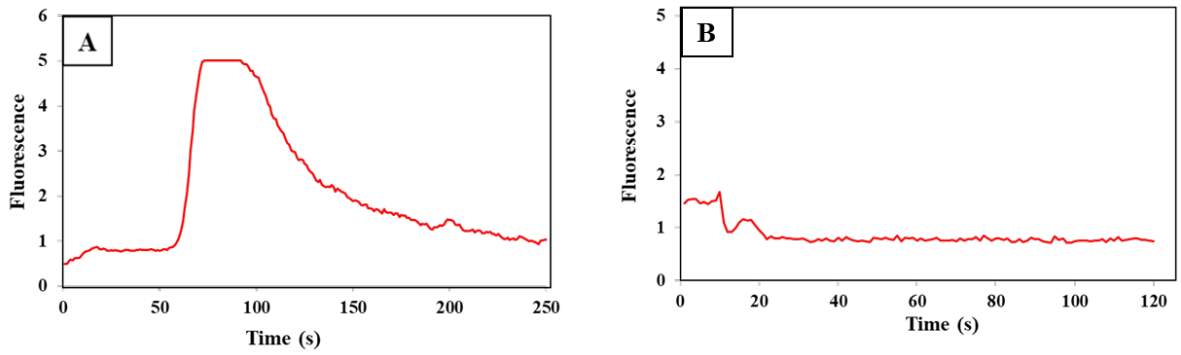

Figure 3.4 Fluorescence elution profiles of (A) 50 nM AF532-labeled ferritin on a polyclonal anti-lactoferrin column and (B) 300 nM AF532-labeled CRF on a polyclonal anti-ferritin column.

3.3.3 BLI of PTB Biomarkers and Their Target Polyclonal Antibodies

Even with the observed cross reactivity issues, I decided to obtain K_d data for three PTB biomarkers with their polyclonal antibodies. Figure 3.5 shows the fitting curves for association and dissociation for ferritin, lactoferrin, and CRF and their respective polyclonal antibodies at different concentrations. The K_d values for the three PTB biomarkers were calculated for their polyclonal antibodies as seen in Table 3.2. These data show that, of these three, lactoferrin has the strongest binding affinity toward its anti-lactoferrin antibody, and CRF has the lowest binding affinity toward anti-CRF. If these three biomarkers are loaded together onto a multiplexed affinity column, I expect that CRF should dissociate more readily from its target, followed by ferritin and then lactoferrin.

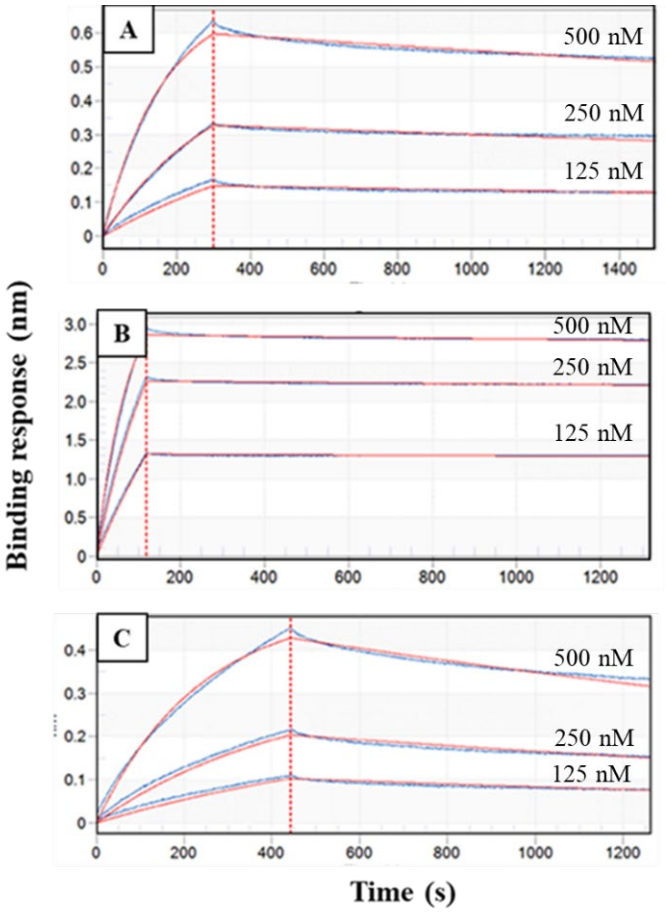

Figure 3.5 BLI association and dissociation data and fitting for ferritin, lactoferrin, and CRF binding to their respective polyclonal antibodies. (A) Anti-ferritin, (B) anti-lactoferrin and (C) anti-CRF at different concentrations. The red curves are the antibody with different concentrations and the blue curves are the control reference.

The K_d values in Table 3.2 are in the nanomolar range for ferritin, lactoferrin, and CRF, as expected for polyclonal antibodies.[18] For lower affinity antibodies (higher K_d), it may be difficult to detect the antigen if present at a low concentration in serum. For example, the PTB risk level in blood serum for ferritin is 0.040 nM, which is more than 200x lower than the K_d of polyclonal anti-ferritin (10 nM). To effectively extract ferritin from blood serum at PTB risk levels, I will need to increase the antibody concentration or increase the affinity. One way to access lower biomarker concentrations would be to alter the K_d by using another antibody that has higher affinity to the antigen. This same approach can be applied for the rest of the PTB biomarkers.

Table 3.2 Calculated K_d values of polyclonal anti-ferritin, anti-lactoferrin, and anti-CRF binding to ferritin, lactoferrin, and CRF via BLI assay**.**

PTB Biomarkers	K_d (nM)
Ferritin and anti-ferritin	9.9
Lactoferrin and anti-lactoferrin	2.7
CRF and anti-CRF	47

3.4. Characterization of Monoclonal Antibodies

Because there was cross reactivity between PTB biomarkers and off-target polyclonal antibodies, I conducted dot blot analysis for monoclonal antibodies. Monoclonal antibodies have the ability to recognize a specific epitope on the antigen, so I expected no cross reactivity between PTB biomarkers and off-target antibodies.

Figure 3.6 shows three replicates dot blots in each panel. Figure 3.6A is a positive control between ferritin and anti-ferritin. Figure 3.6B shows binding between ferritin and a monoclonal ferritin antibody, while Figure 3.6C shows interaction between lactoferrin and monoclonal anti-lactoferrin. Figure 3.6D displays fluorescent dots for peptide 2 and anti-ITIH4, which indicates binding between them. Similarly, Figure 3.6E demonstrates binding between peptide 3 and anti-ITIH4. These dot blots show successful binding between monoclonal antibodies and their respective PTB biomarkers, which makes them a great choice to use in immunoaffinity extraction.

Cross reactivity was further studied between ferritin and lactoferrin toward off target monoclonal antibodies. No binding was observed between ferritin and monoclonal anti-lactoferrin as seen in Figure 3.6F. In Figure 3.6G, no fluorescence was observed between lactoferrin and monoclonal anti-ferritin. No fluorescent dots were seen in either Figure 3.6H or I

when ferritin was dotted on either monoclonal anti-CRF or monoclonal anti-TNF. The lack of cross reactivity gives additional support to the ability to use these monoclonal antibodies for multiplex immunoaffinity experiments.

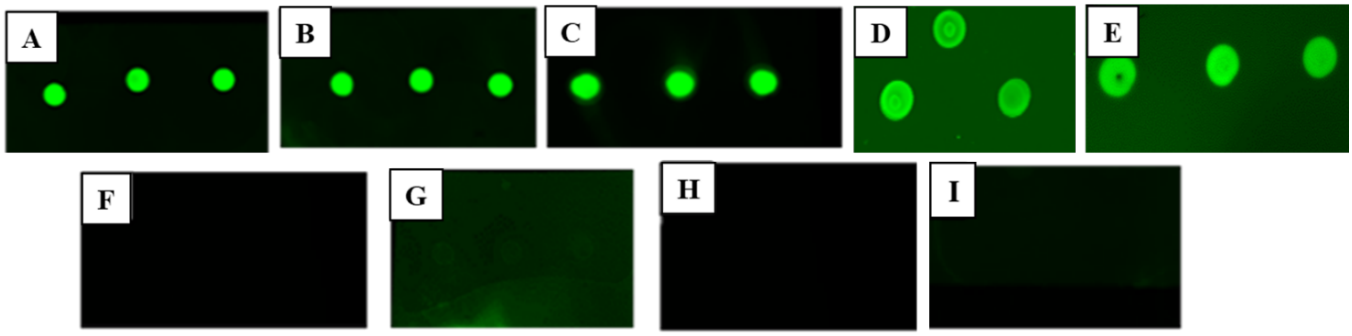

Figure 3.6 Dot blot assays on nitrocellulose membranes for monoclonal antibodies. Three duplicate dots of (A) positive control with ferritin and anti-ferritin. (B) Ferritin and mAb anti-ferritin. (C) Lactoferrin and mAb anti-lactoferrin. (D) Peptide 2 and anti-ITIH4. (E) Peptide 3 and anti-ITIH4. (F) Ferritin and mAb anti-lactoferrin. (G) Lactoferrin and mAb anti-ferritin. (H) Ferritin and mAb anti-CRF. (I) Ferritin and mAb anti-TNF.

3.5 Immunoaffinity Extraction of PTB Biomarkers Using Monoclonal Antibodies

After I characterized monoclonal antibodies to ferritin, lactoferrin, peptide 2, and peptide 3 and verified the lack of off-target binding, I developed individual immunoaffinity columns for extraction of three of these PTB biomarkers in 3D printed microfluidic devices. These studies lay the foundation for subsequent extraction of multiple PTB biomarkers on a multiplexed immunoaffinity column. Figure 3.7A-B each shows an elution peak at 20 seconds for ferritin and lactoferrin from their respective monoclonal antibody column compared to a blocked column. Ferritin has a narrow and taller peak on the affinity column compared to the blocked column. In contrast, lactoferrin shows a wider peak and a little increase in the fluorescence at 10 seconds, which may indicate adsorption of lactoferrin to the monolith. Figure 3.7C shows a slightly taller and wider elution peak that appears at 20 seconds for peptide 2 loaded from buffer on an anti-ITIH4 column, compared to the narrower signal observed on a control column. Figure 3.7D

shows a wider elution peak that appears at 60 seconds for loaded peptide 2 spiked in blood serum for an antibody column, compared to little elution seen for the same sample loaded on a blocked monolith. These data indicate successful retention and elution of two PTB protein biomarkers, ferritin and lactoferrin from buffer, as well as successful elution of peptide 2 from anti-ITIH4 column when loaded from either buffer or blood serum.

Only a little off-target binding was seen when the PTB biomarker ferritin was loaded on either monoclonal anti-lactoferrin or anti-TNF, as seen in Figure 3.8A-B. This binding may result from non-specific adsorption from ferritin to the immunoaffinity column, and not from binding of ferritin to off-target monoclonal antibodies, consistent with dot blot data in Figure 3.6.
These experiments show successful development of immunoaffinity columns for PTB biomarker extraction from their respective monoclonal antibodies. Monoclonal antibodies for three other PTB biomarkers, CRF, TNF, and TAT are further characterized, immobilized, and used for multiplexed extraction from a single immunoaffinity column as discussed in chapter 4.

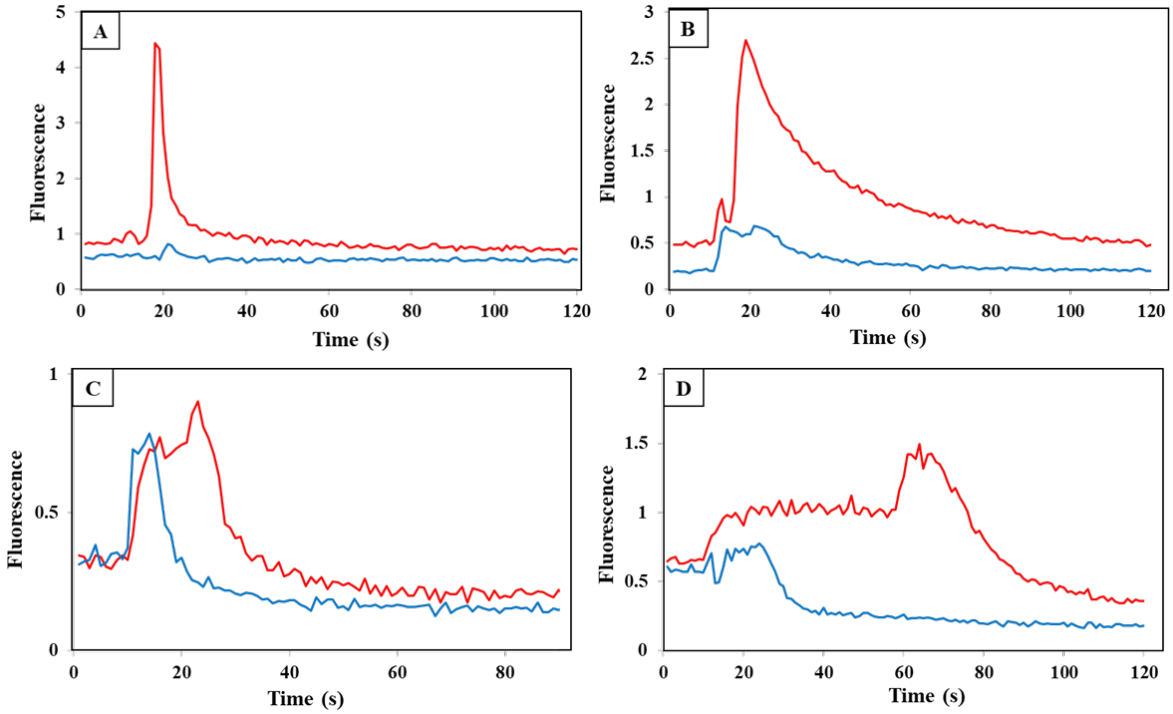

Figure 3.7 Fluorescence during elution after extraction of AF532-labeled PTB biomarkers from a monoclonal antibody-modified column (red) or a control monolith lacking attached antibody (blue) for (A) 50 nM ferritin and (B) 100 nM lactoferrin in 20 mM phosphate buffer pH 7, or (C) 500 nM peptide 2 in either (C) buffer or (B) human blood serum diluted 5-fold in phosphate buffer pH 8.

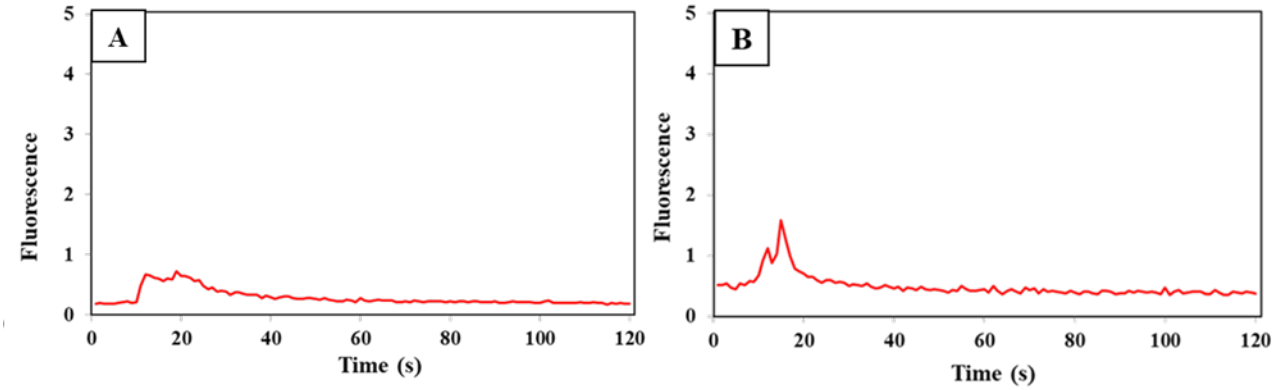

Figure 3.8 Fluorescence elution profiles of (A) 50 nM AF532-labeled ferritin on a monoclonal anti-lactoferrin and (B) a monoclonal anti-TNF column.

3.6 Conclusions

I was successful in finding polyclonal antibodies to target multiple PTB biomarkers. I also developed a polyclonal immunoaffinity column to extract the PTB protein biomarker lactoferrin, in a 3D printed microfluidic device. I was able to test cross reactivity between PTB biomarkers and multiple off-target polyclonal antibodies. Substantial off-target binding between PTB protein biomarkers and polyclonal antibodies was seen, while a lack of off-target interaction was observed between PTB peptide biomarkers and polyclonal antibodies.

I used a BLI assay to study the binding affinity between ferritin, lactoferrin, and CRF and their polyclonal antibodies. The K_d values calculated were in the nanomolar range as expected for polyclonal antibodies.[18] Measuring the K_d values for the remaining PTB biomarkers will allow us to determine which of the biomarkers dissociates more readily from its target in a multiplexed immunoaffinity experiment. High affinity antibodies will increase my ability to easily target PTB biomarkers at lower concentrations in blood serum.

Initial experiments with monoclonal antibodies showed good binding affinity with their target biomarker and no off-target binding between any of the studied PTB biomarkers and monoclonal antibodies. This makes them an ideal option for extracting multiple PTB biomarkers in a multiplex immunoaffinity column. I found compatible monoclonal antibodies for ferritin, lactoferrin, peptide 2, and peptide 3. I also developed an immunoaffinity column to retain and extract three PTB biomarkers, ferritin, lactoferrin, and peptide 2 using their monoclonal antibodies in 3D printed microfluidic devices. Building further on work described in Chapter 4, in the future it may be possible to immobilize monoclonal antibodies for all nine PTB biomarkers in immunoaffinity columns and extract PTB biomarkers from human blood serum.

3.7 References

1. Oss, C. J. V. Hydrophobic, Hydrophilic and other Interactions in epitope-paratope binding. *Mol. Immunol.* **1995,** *32*, 199-211.

2. Wilson, J. H.; Hunt, T.; *Molecular biology of the cell, 4th edition: a problems approach*. Garland Science: New York; London, **2002**.

3. Lipman, N. S.; Jackson, L. R.; Trudel, L. J.; and Weis-Garcia, F. Monoclonal Versus Polyclonal Antibodies: Distinguishing Characteristics, Applications, and Information Resources. *ILAR. Journal.* **2005,** *46*, 258-268.

4. Andrade, P.; Narvekar, P.; Montoya, M.; Michlmayr, D.; Balmaseda, A.; Coloma, J.; Harris, E. Primary and Secondary Dengue Virus Infections Elicit Similar Memory B-Cell Responses, but Breadth to Other Serotypes and Cross-Reactivity to Zika Virus Is Higher in Secondary Dengue. *J. Infect. Dis.* **2020,** *222*, 590-600.

5. Moreno, I.; Dominguez, M.; Torano, A. A kinetic ELISA to determine the immunoreactive fraction of monoclonal antibodies. *J. Immunol. Methods.* **2020,** *476*, 112689.

6. Chatterjee, T.; Knappik, A.; Sandford, E.; Tewari, M.; Choi, S. W.; Strong, W. B.; Thrush, E. P.; Oh, K. J.; Liu, N.; Walter, N. G.; Johnson-Buck, A. Direct kinetic fingerprinting and digital counting of single protein molecules. *Proc. Natl. Acad Sci. U.S.A.* **2020,** *117*, 22815-22822.

7. Torano, A.; Moreno, I.; Infantes, J. A.; Dominguez, M. Development of a competitive inhibition kinetic ELISA to determine the inhibition constant (Ki) of monoclonal antibodies. *J. Immunol. Methods.* **2021,** *493*, 113042.

8. Prasad, P. V.; Rani, A.; Chaube, S. K.; Rohil, V.; Shrivastav, T. G. Kinetic analysis of a human chorionic gonadotropin-beta epitope-paratope interaction. *Growth Factors.* **2008,** *26*, 331-42.

9. Livingstone, J. R. Antibody characterization by isothermal titration calorimetry. *Nature,* **1996,** *384*, 491-492.

10. Tighe, P. J.; Ryder, R. R.; Todd, I.; Fairclough, L. C. ELISA in the multiplex era: potentials and pitfalls. *Proteomics Clin Appl.* **2015,** *9*, 406-22.

11. Karlsson, R.; Michaelsson, A.; Mattsson, R. Kinetic analysis of monoclonal antibody-antigen interactions with a new biosensor based analytical system. *J. Immunol. Methods.* **1991,** *145, 229-240*.

12. Abdiche, Y.; Malashock, D.; Pinkerton, A.; Pons, J. Determining kinetics and affinities of protein interactions using a parallel real-time label-free biosensor, the Octet. *Anal. Biochem.* **2008,** *377*, 209-17.

13. Estep, P.; Reid, F.; Nauman, C.; Liu, Y.; Sun, T.; Sun, J.; Xu, Y. High throughput solution-based measurement of antibody-antigen affinity and epitope binning. *MAbs.* **2013,** *5*, 270-8.

14. Kamat, V.; Rafique, A.; Huang, T.; Olsen, O.; Olson, W. The impact of different human IgG capture molecules on the kinetics analysis of antibody-antigen interaction. *Anal. Biochem.* **2020,** *593*, 113580.

15. Vala, M.; Jordan, L. R.; Warrington, A. E.; Maher, L. J., 3rd; Rodriguez, M.; Wittenberg, N. J.; Oh, S. H. Surface Plasmon Resonance Sensing on Naturally Derived Membranes: A Remyelination-Promoting Human Antibody Binds Myelin with Extraordinary Affinity. *Anal. Chem.* **2018,** *90*, 12567-12573.

16. Nielsen, J. B.; Nielsen, A. V.; Carson, R. H.; Lin, H. L.; Hanson, R. L.; Sonker, M.; Mortensen, D. N.; Price, J. C.; Woolley, A. T. Analysis of thrombin-antithrombin complex formation using microchip electrophoresis and mass spectrometry. *Electrophoresis.* **2019,** *40*, 2853-2859.

17. Parker, E. K.; Nielsen, A. V.; Beauchamp, M. J.; Almughamsi, H. M.; Nielsen, J. B.; Sonker, M.; Gong, H.; Nordin, G. P.; Woolley, A. T. 3D printed microfluidic devices with immunoaffinity monoliths for extraction of preterm birth biomarkers. *Anal. Bioanal. Chem.* **2019,** *411*, 5405-5413.

18. Torres, O. B.; Duval, A. J.; Sulima, A.; Antoline, J. F. G.; Jacobson, A. E.; Rice, K. C.; Alving, C. R.; Matyas, G. R. A rapid solution-based method for determining the affinity of heroin hapten-induced antibodies to heroin, its metabolites, and other opioids. *Anal. Bioanal. Chem.* **2018,** *410*, 3885-3903.

4. IMMUNOAFFINITY MONOLITHS FOR MULTIPLEXED EXTRACTION OF PRETERM BIRTH BIOMARKERS FROM HUMAN BLOOD SERUM IN 3D PRINTED MICROFLUIDIC DEVICES*

4.1 Introduction

Multiplexed assays are important for drug screening,[1] cytotoxicity,[2] and biomarker detection.[3-4] Biomarkers can serve as indicators for the presence of disease, but are usually present in low concentrations in blood serum.[5] Particularly, because blood serum contains up to 50 g/L of albumin and immunoglobulins,[6] these matrix components can interfere with biomarker analysis, making biomarker detection a challenging endeavor.[7]

Risk for a preterm birth (PTB), defined as birth prior to 37 weeks of gestation, can be correlated with a panel of nine biomarkers found in maternal blood serum.[8] These biomarkers include four proteins and five peptides, and allow for prediction of PTB risk with 87% selectivity and 81% specificity. However, detecting these biomarkers from human blood serum is challenging due to their very low concentrations relative to other proteins in serum. To achieve successful early diagnosis of PTB risk, there is a need for effective and rapid sample preparation methods to address these issues.

---

* This chapter is adapted from:
Almughamsi, H. M.; Howell, K. M.; Parry, S. R.; Esene, J. E.; Nielsen, J. B.; Nordin, G. P.; Woolley, A. T. Immunoaffinity Monoliths for Multiplexed Extraction of Preterm Birth Biomarkers from Human Blood Serum in 3D Printed Microfluidic Devices. *Analyst*. Submitted

An immunoaffinity column selectively retains analytes using antigen-antibody interaction. This strong and selective interaction is desirable for purifying target biomarkers from complex specimens. Porous polymer monoliths are useful in sample preparation[9-11] and show promise in immunoaffinity extraction of biomarkers in blood using one or more antibodies attached to a column.[12-13] The biophysical characteristics of antigen-antibody binding play a significant role in immunoaffinity extraction. Understanding this interaction provides information about the stability of binding, which is useful for development of multiplexed immunoaffinity extraction. Biolayer interferometry (BLI)[14] and surface plasmon resonance (SPR)[15] are powerful, label-free methods that are used to determine affinity binding strength between antigen-antibody complexes.

Microfluidics is a promising platform for multiplex sample preparation. The small amounts of sample and reagents needed can reduce costs and analysis time.[16-17] 3D printing of microfluidic devices can overcome challenges associated with traditional fabrication techniques, and can enable novel designs that are otherwise inaccessible.[12,18-21] These 3D printed microfluidic devices can be used to facilitate sample preparation and biomarker analysis. For example, Bickham et al.[19] used solid phase extraction monoliths to concentrate and label a panel of nine PTB biomarkers. Although this is a good method for enriching and labeling samples, PTB biomarkers have to be first purified from blood serum, which cannot be performed on this type of monolith. Parker et al.[12] purified ferritin from human blood serum as a step toward a PTB risk diagnostic, but only one PTB biomarker was captured on a single-antibody column. Thus, extending this approach to immobilize multiple antibodies and extract multiple PTB biomarkers on a single immunoaffinity column would be advantageous for point-of-care testing.[22]

Here, I overcome these earlier limitations with immunoaffinity columns to purify multiple PTB biomarkers simultaneously from human blood serum in 3D printed microfluidic devices. Immunoaffinity columns were modified with a mixture of monoclonal antibodies that were initially evaluated using dot blots, BLI, and SPR. Selectivity of each biomarker toward its respective antibody was first studied, and each biomarker was individually extracted from a single-antibody column. I then selectively enriched three PTB biomarkers from blood serum using multiplexed immunoaffinity monoliths in 3D printed microfluidic devices. This study is the first use of a well-characterized, high-specificity immunoaffinity column that simultaneously extracts several PTB biomarkers in a 3D printed microfluidic device. This is a key step toward the future development of 3D printed microfluidic devices for rapid PTB risk assessment.

4.2 MATERIALS AND METHODS

4.2.1 Chemicals

Glycidyl methacrylate (GMA), ethylene glycol dimethacrylate (EDMA), 1-dodecanol, 2,2-dimethoxy-2-phenylacetophenone (DMPA), poly (ethylene glycol) diacrylate (PEGDA, MW 250), Tris hydrochloride, 3-(trimethoxysilyl) propyl methacrylate, dimethyl sulfoxide (DMSO), phenylbis (2,4,6 trimethylbenzoyl) phosphine oxide (Irgacure 819), Amicon ultra 0.5-mL centrifugal filters (10 and 50 kDa cutoff), boric acid, sodium bicarbonate, and sodium carbonate were obtained from ThermoFisher (St. Louis, MO). Alexa Fluor 532 (carboxylic acid, succinimidyl ester) and Tris base were purchased from Fisher Scientific (Fair Lawn, NJ). Solutions were made using deionized water (18.3 MΩ) filtered by a Barnstead EASY-pure UV/UF system (Dubuque, IA). Isopropyl alcohol (IPA) was from Macron (Center Valley, PA). Cyclohexanol was obtained from Spectrum (New Brunswick, NJ). 2-Nitrophenyl phenyl sulfide (NPS) came from TCI (Portland, OR). Amicon ultra-4 centrifugal filters (15 mL, 10 and 30 kDa

cutoff), and 4-(2-hydroxyethyl)-1-piperazineethanesulfonic acid (HEPES) were purchased from EMD Millipore (Billerica, MA). Glass slides for 3D printing were purchased from VWR (Radnor, PA).

4.2.2 Biological Components

Corticotropin releasing factor (CRF) came from GenScript (Piscataway, NJ), and tumor necrosis factor-α receptor type 1 (TNF) was purchased from ProSpec (East Brunswick, NJ). Thrombin and antithrombin were obtained from Haematologic Technology (Essex Junction, VT), and heparin was obtained from Alfa-Aesar (Haverhill, MA). Antibodies to thrombin-antithrombin complex (anti-TAT, produced in mice) were purchased from Abcam (Cambridge, MA). Anti-CRF (produced in mice), anti-TNF (produced in mice), EZ-Link Sulfo-NHS-LC-Biotin, and high select top 14 abundant protein depletion midi spin columns were obtained from ThermoFisher (St. Louis, MO). Dry milk was purchased from Walmart (Bentonville, AR). Nitrocellulose paper was obtained from Bio-Rad (Hercules, CA), and IRDye 800CW labeled secondary goat anti-mouse IgG came from LICOR (Lincoln, NE). Female human blood serum (off-the-clot, sterile filtered) was purchased from Zen-Bio (Research Triangle Park, NC). Streptavidin biosensors were purchased from ForteBio (Fremont, CA) and bovine serum albumin (BSA) was purchased from EMD Millipore.

4.2.3 3D Printed Microfluidic Devices

The microfluidic devices (Figure 4.1A) were adapted from Bickham et al.[19] and designed to have five separated channels, each with a 50 μm x 45 μm cross section. Each channel had a reservoir on one side of the device and a port in the other side for PTFE tubing (0.22 in ID x 0.042 in OD; Cole Parmer, Vernon Hills, IL) to connect to vacuum and flow analyte through the

channel. A 600 µm wide monolith polymerization window (MPW) was designed in each device to allow monolith polymerization.[12] 97% PEGDA, 2% NPS UV absorber, and 1% Irgacure 819 photoinitiator composed the resin used to fabricate the devices in a custom 3D printer.[23]

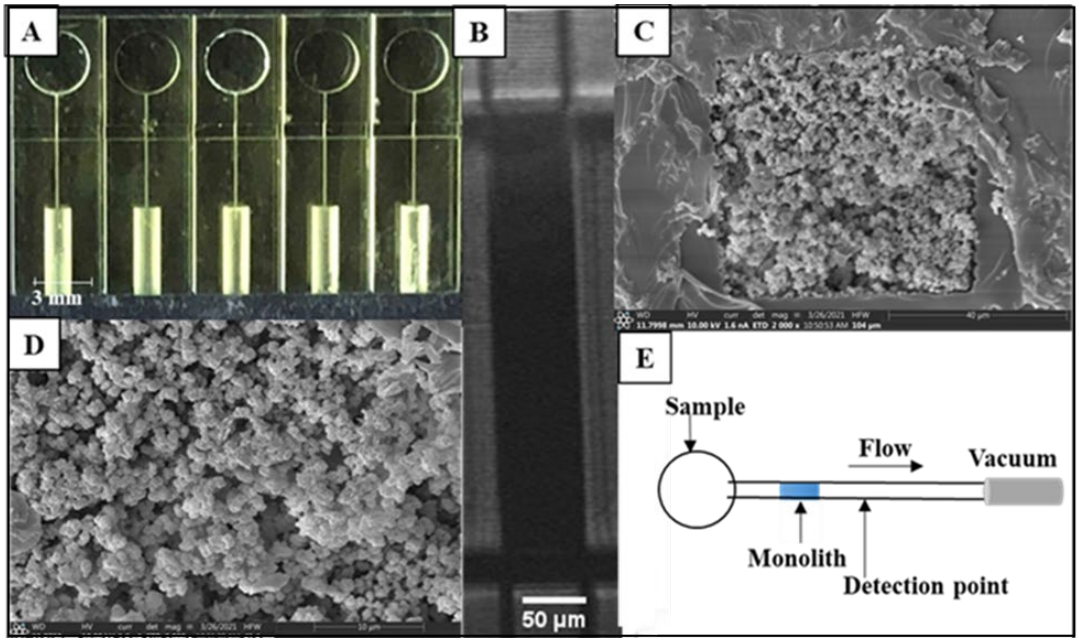

Figure 4.1 3D printed devices with monoliths for affinity extraction. (A) Photograph of 3D printed device. (B) Photograph of monolith inside channel. (C-D) SEM images of monoliths prepared in a 3D printed microfluidic device; (C) channel view and (D) zoom view. (E) Device schematic for PTB biomarker extraction. The labeled biomarker flows through the channel via vacuum; as labeled analytes pass the detection point, the signal is recorded.

4.2.4 PTB Biomarker Preparation

The PTB biomarkers were fluorescently labeled; CRF and TNF were dissolved in 10 mM bicarbonate buffer (BCB, pH 10), and TAT was prepared as in Nielsen et al.[24] Alexa Fluor 532 was dissolved in DMSO, added to each biomarker and incubated at room temperature overnight. CRF (100 µM), TNF (40 µM), and TAT (26 µM), were labeled at a dye:biomarker molar ratio of 3:2, 20:1 and 20:1, respectively. Next, TNF and TAT were filtered four times at 14,000 RPM for

15 min using a 10-kDa or 50-kDa cutoff filter, respectively, to remove excess dye. Samples were diluted to the desired concentration in 20 mM HEPES buffer pH 7. To prepare depleted blood serum, I followed the Thermo Fisher protocol for their columns (Cat No. A36371). Briefly, 100 µL of serum was added into a pre-filled midi spin column that contained 1000 µL of a 50% slurry in 10 mM PBS, 0.02% sodium azide, pH 7.4. Then, the column was gently inverted to form a homogenous mixture, which was incubated in the column for 10 min with gentle agitation. I placed the column in a 15 mL falcon tube and centrifuged the column at 1000 g for 2 min. Afterward, the depleted serum, now 10-fold diluted, was collected and stored at -20ºC until further use. Labeled biomarker samples were spiked into the depleted serum to yield 100 nM CRF, 30 nM TNF, and 60 nM TAT.

4.2.5 Kinetic Characterization

K_d values were calculated for CRF, TNF, and TAT with their respective monoclonal antibodies. Assays were conducted using either Biacore (Creative Biolabs) SPR (CRF and TNF) or an OCTET RED96 biolayer interferometer (ForteBio) in PBS pH 7 at 30 ºC with 1000 rpm shaking (TAT). TAT was biotinylated as described in the ThermoFisher protocol for product No. A39257. Then, the BLI assay was run on a standard microwell plate when the streptavidin biosensors were loaded with the biotinylated TAT at 5-10 µg/mL at 300 s. Five sensors were used, three for antibody binding, and two for the reference control. The loaded sensors were equilibrated first with PBS pH 7 to generate the baseline. Then, the association step was performed 30 s for different concentrations ranging from 62 to 250 nM. The dissociation step was performed in the assay buffer for 800 s in PBS pH 7. The data for association and dissociation were analyzed by Octet Data Analysis 8.2 software and fit to a 1:1 binding model to obtain kinetic parameters. SPR data were obtained on samples shipped to Creative Biolabs.

4.2.6 Monolith Formation

Modified monoliths were prepared as reported by Parker et al.[12] using 24% GMA as the monomer, 11% EDMA as cross linker, 10% cyclohexanol and 55% 1-dodecanol as porogens, and 1% DMPA as the photoinitiator. The monolith mixture was sonicated for 10 min and loaded into the microfluidic channel via capillary action. Then, the entire device was placed under a UV light (SunRay 600, Uvitron, West Springfield, MA) for 10 min allowing the monolith to polymerize at the desired channel location in the MPW. After polymerization, PTFE tubing was inserted into the device port and hot glued in place. The unpolymerized mixture was removed from the channel by flushing with IPA for 30 min using vacuum. Scanning electron microscopy (SEM) images of the monolith were taken by removing the 3D-printed channel from the glass slide using a razor blade. Then, the monoliths were cut through the MPW and affixed on stubs using carbon tape. Next, 80:20 Au:Pd was sputter coated on the surface of the monolith using a Q150 T ES Sputterer (Quorum Technologies, Lewes, East Sussex, UK). Finally, the SEM images were taken using an Apreo C Low-Vacuum SEM instrument (Thermo) in high vacuum mode at 10 kV.

4.2.7 Antibody Immobilization

Compatibility of the PTB biomarker antibodies towards their targets and off-target analytes was tested using dot blots. Solutions of CRF, TNF, and TAT (2 µL, 1 mg/ml) were dotted on nitrocellulose paper and left to dry for 30 min. Then, a blocking buffer of either 5% milk, or 5% BSA in 10× Tris buffer saline (TBS) was applied for 1 h to prevent nonspecific binding. Next, primary antibodies (1 µg/mL in TBS plus 0.05% Tween 20; TBST) were added and incubated for 1 h for binding to the biomarker. TBST was used to rinse away unbound antibodies for 15 min. Finally, the labeled secondary antibody (1 µg/mL in TBS) was incubated

for 1 h, and the paper was washed again with TBST for 15 min. The dot blots were scanned via a LI-COR ODYSSEY imaging system. The cross reactivity between each antibody and off-target biomarker was also tested using the process above.

The attachment of each antibody to the GMA monolith was verified using fluorescence images. To measure attachment to monoliths anti-CRF, anti-TNF, and anti-TAT were labeled at a dye:antibody molar ratio of 10:1 and were filtered four times at 14,000 RPM for 15 min using a 10-kDa cutoff filter to remove excess dye. I directed a 532 nm laser through a 4X objective and captured images with a Hamamatsu ORCA-Fusion CMOS camera (Bridgewater, NJ) using 10, 100, or 300 ms exposure times. First, a blank image of the monolith was taken before attaching the antibody. Then, the monoclonal anti-CRF, anti-TNF, or anti-TAT labeled with Alexa Fluor 532 was immobilized onto the monolith overnight. Next, the monolith was rinsed with 20 mM borate buffer pH 8 for 30 min and another monolith image was captured. Background-subtracted fluorescence of the monolith with the labeled antibody and the control channel was determined using Image J (imagej.nih.gov). To measure the background-subtracted fluorescence for extracted PTB biomarkers, the same steps were used with monolith images taken at each stage of the experimental process: loading, rinsing, and elution. Fluorescence values were normalized to the signal after loading, and the average signal was determined from three replicates.

For the attachment of the multiple antibodies to the monolith, a mixture consisting of 4 µL each of anti-CRF, anti-TNF, and anti-TAT (1 mg/mL) was added to the device and allowed to flow through the channel via capillary action. 20 mM borate buffer pH 8 was next added to the reservoirs and the entire device was covered with parafilm and placed in a humid chamber overnight to prevent the channel from drying. This reaction time allowed amine groups in the antibody to bind covalently to the epoxy groups in the immunoaffinity monolith. Following

overnight incubation, 0.1 M Tris buffer (pH 8.5) was flowed through the channel and then incubated for 1 h to block any remaining epoxy groups. Finally, the channel was rinsed with 20 mM HEPES buffer pH 7 for 5 min. For control experiments, the monolith was blocked using Tris buffer and no antibodies were incubated.

4.2.8 Immunoaffinity Extraction

The experimental set up was as follows: a 532 nm laser was used to induce fluorescence. The fluorescence signal was recorded with a photomultiplier tube and digitized using LabVIEW software. Experiments were then carried out in the following steps. First, channels were filled with 20 mM HEPES buffer pH 7 and vacuum was applied for 1 min through the device as seen in Figure 1E. Then, the vacuum was paused, the reservoir was emptied, the fluorescently labeled analyte was loaded into the reservoir, and analyte was drawn through the channel by applying vacuum for ~40 s. The labeled analyte was incubated in the monolith for 10 min, after which the reservoir was washed three times with 20 mM HEPES buffer pH 7, and the monolith had 20 mM HEPES buffer drawn through until the signal went back to baseline. Finally, the reservoir was filled with 50 mM BCB and vacuum was applied for 1 min to elute the sample.

4.3 Results and Discussion

4.3.1 Antibody Characterization

Dot blots were used to confirm the compatibility between CRF, TNF, and TAT and their respective antibodies, as well as their cross reactivity toward off-target antibodies. Figure 4.2 shows three replicate dot blots in each panel. Figure 4.2A displays a positive control for ferritin and anti-ferritin binding. Figure 4.2B-D similarly shows binding between CRF and anti-CRF, TNF and anti-TNF, and TAT and anti-TAT. Figure 4.2E shows that binding also occurs between thrombin and anti-TAT. No binding was observed between antithrombin and anti-TAT as seen in

Figure 4.2F. I hypothesize that rather than affinity interaction, thrombin nonspecifically sticks to primary antibodies, and in Figure 4.2G, I confirmed that thrombin also binds non-specifically to anti-ferritin. These dot blots demonstrate that the anti-CRF, anti-TNF, and anti-TAT antibodies selected are appropriate for CRF, TNF, and TAT, and that thrombin by itself may stick nonspecifically to antibodies.

I further studied the cross reactivity between CRF, TNF, and TAT, and off-target antibodies, as shown in the dot blots in Figure 4.2H-M. No fluorescent dots were seen in any of these experiments, which confirmed a lack of affinity binding between CRF, TNF, and TAT, and off-target antibodies. These data further support the use of these anti-CRF, anti-TNF, and anti-TAT antibodies for multiplex immunoaffinity experiments.

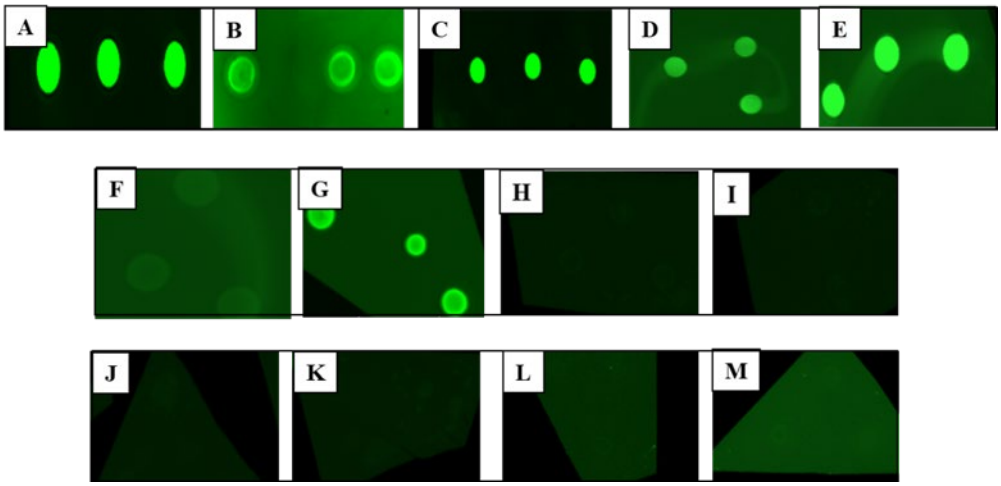

Figure 4.2 Dot blot assays on nitrocellulose membranes. Three duplicate dots of (A) positive control with ferritin and anti-ferritin; (B) CRF and anti-CRF; (C) TNF and anti-TNF; (D) TAT and anti-TAT; (E) thrombin and anti-TAT; (F) antithrombin and anti-TAT; (G) Thrombin and anti-ferritin. (H) CRF and anti-TNF; (I) CRF and anti-TAT; (J) TAT and anti-TNF; (K) TAT and anti-CRF; (L) TNF and anti-TAT; (M) TNF and anti-CRF.

4.3.2 SPR and BLI of PTB Biomarkers with their Target Monoclonal Antibodies

I obtained K_d data for CRF, TNF, and TAT with their monoclonal antibodies using either SPR or BLI. Figure 4.3 shows the fitting curves for association and dissociation of CRF, TNF,

and TAT with their corresponding antibodies. The K_d values for these three PTB biomarkers and their monoclonal antibodies were calculated as seen in Table 4.1. The K_d values in Table 4.1 show that of these three, TAT has the strongest binding affinity toward its antibody, and CRF has the lowest binding affinity toward anti-CRF. This means in a multiplex affinity column, CRF will dissociate more readily from its target compared to TNF and TAT. The lower affinity for CRF and anti-CRF likely is due to the smaller size of CRF, relative to TNF and TAT.

Table 4.1 K_d values for monoclonal anti-CRF, anti-TNF, and anti-TAT binding to their antigen.

PTB Biomarkers	**K_d (nM)**
CRF and anti-CRF	41
TNF and anti-TNF	1.4
TAT and anti-TAT	0.11

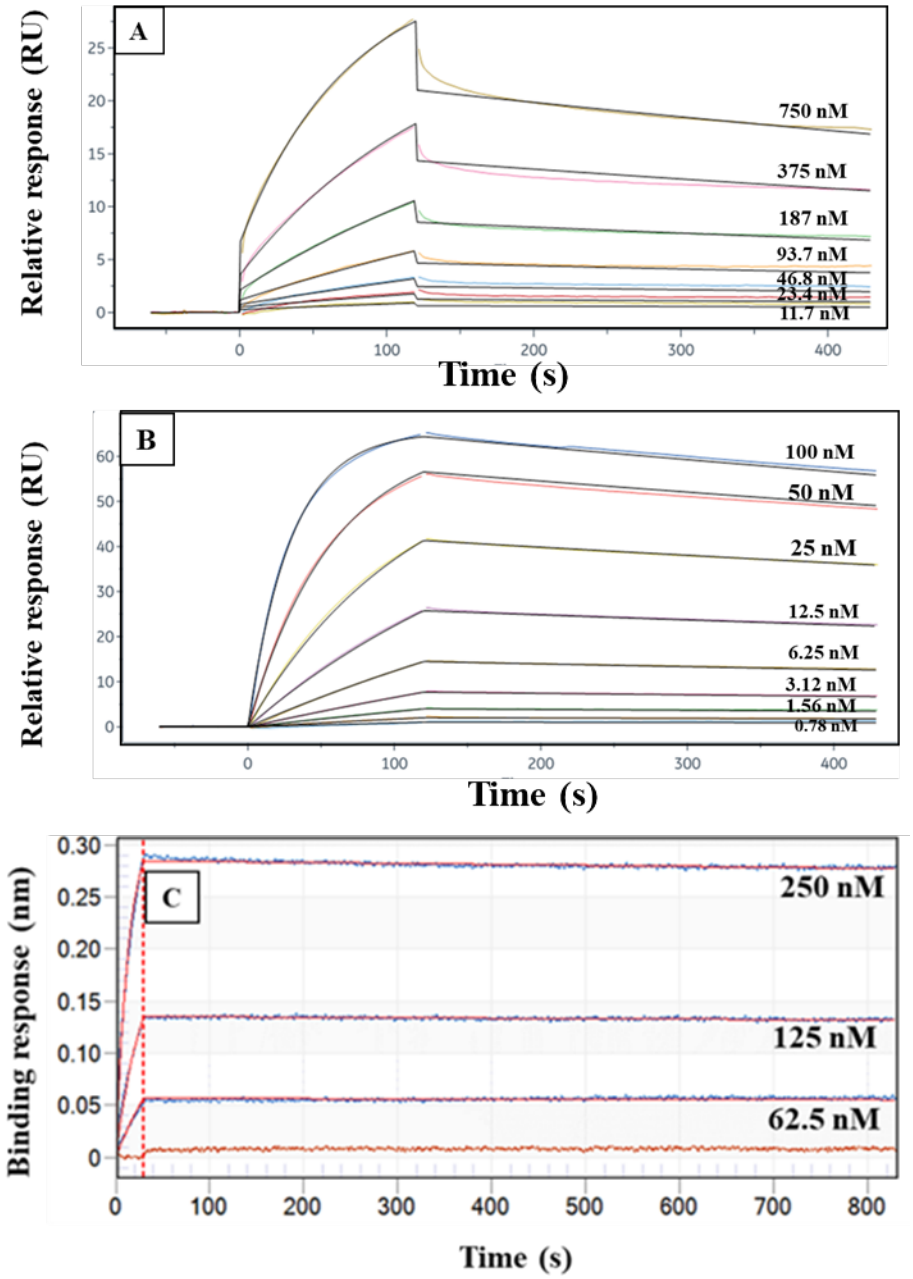

Figure 4.3 Association and dissociation data and fitting for CRF, TNF, and TAT binding to their respective monoclonal antibodies. CRF and TNF data were collected from SPR. TAT data were obtained with BLI. Different concentrations of (A) CRF, (B) TNF, or (C) anti-TAT.

4.3.3 Monolith Characterization and Modification

I used the same monolith formulation that Parker et al.[12] developed to retain the PTB biomarker, ferritin, using a single-antibody column. GMA monoliths were successfully formed

inside channels as seen in Figure 4.1B. The morphology of a representative monolith was determined using SEM as shown in Figure 4.1C-D. The SEM data in Figure 4.1C show that the monolith is fully attached to the microfluidic channel wall. The monolith pores are randomly distributed as seen in Figure 4.1D, and there is sufficient surface area for antibody immobilization. I analyzed the pore and nodule sizes for my monoliths, which were 0.5 μm ± 0.1 μm (n=30) and 0.7 μm ± 0.1 μm (n=30), respectively.

I used fluorescence imaging to verify the attachment of antibodies to the affinity monoliths, as seen in Figure 4.4. In the control monoliths in Figure 4.4A, C, and E the fluorescence was much lower compared to the fluorescence observed when labeled anti-CRF, anti-TNF, or anti-TAT was attached to the column in Figure 4.4B, D, and F. Figure 4.4G-I shows the background-subtracted fluorescence on the monolith before and after antibody attachment; fluorescence signal significantly increased for labeled anti-CRF, anti-TNF, and anti-TAT columns compared to the control columns. This clear increase in fluorescence confirmed the attachment of antibodies to PTB biomarkers on monoliths.

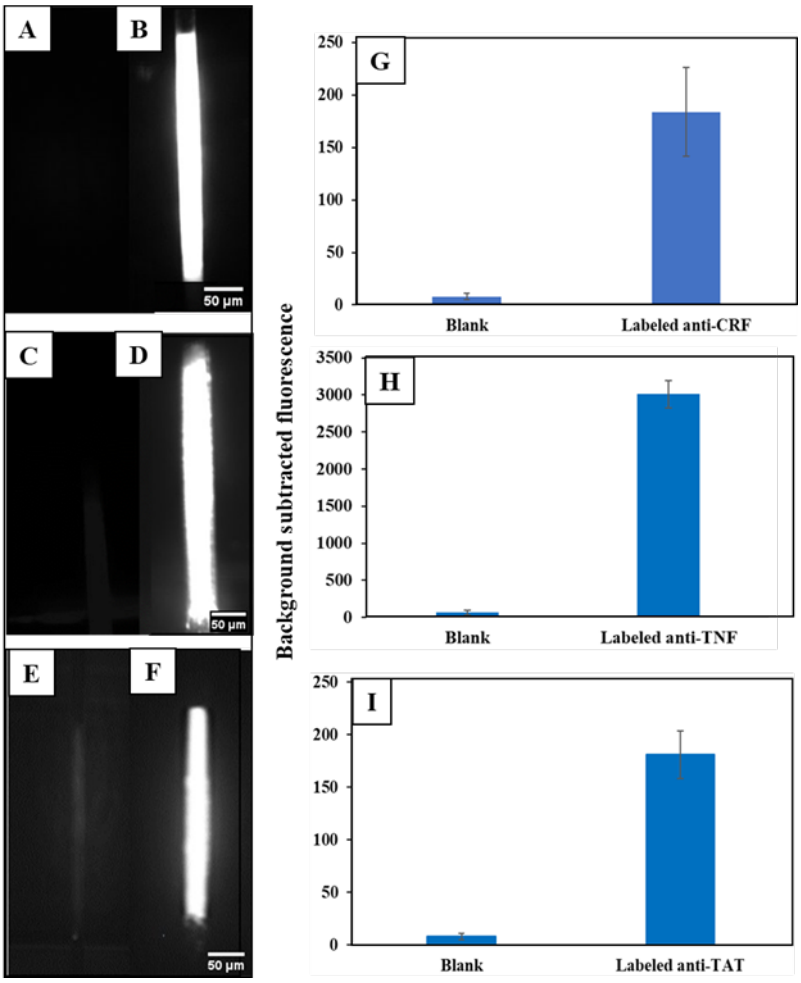

Figure 4.4 Labeled antibody attachment to monoliths. Fluorescence images of (A, C, E) control monoliths and fluorescently labeled monoclonal (B) anti-CRF, (D) anti-TNF, and (F) anti-TAT. Background-subtracted fluorescence of monoliths before and after immobilization of labeled (G) anti-CRF, (H) anti-TNF, and (I) anti-TAT. Error bars show the standard deviation for three replicates.

4.3.4 Immunoaffinity Extraction of PTB Biomarkers

I measured the fluorescence during elution after extraction of CRF, TNF, and TAT on their respective, single-antibody-modified columns and control columns, from both buffer and depleted human blood serum, as seen in Figure 4.5. During the elution step a peak appeared as an increase in fluorescence signal at 5-10 s after flow started for each biomarker loaded from buffer (Figure 4.5A-C). In contrast, little or no increase in the fluorescence signal occurred for the

control monoliths lacking attached antibodies. The elution peaks appeared at similar times for the three biomarkers, but they exhibited different shapes. In the depleted blood serum experiments (Figure 4.5D-F), the elution peaks were seen at 5 s, 15 s, and 20 s for CRF, TNF, and TAT, respectively. These peaks were generally wider and had higher signal compared to the peaks observed for analyte loaded from buffer. These data demonstrate the ability to retain CRF, TNF, and TAT individually on single-antibody columns after loading from either buffer or blood serum.

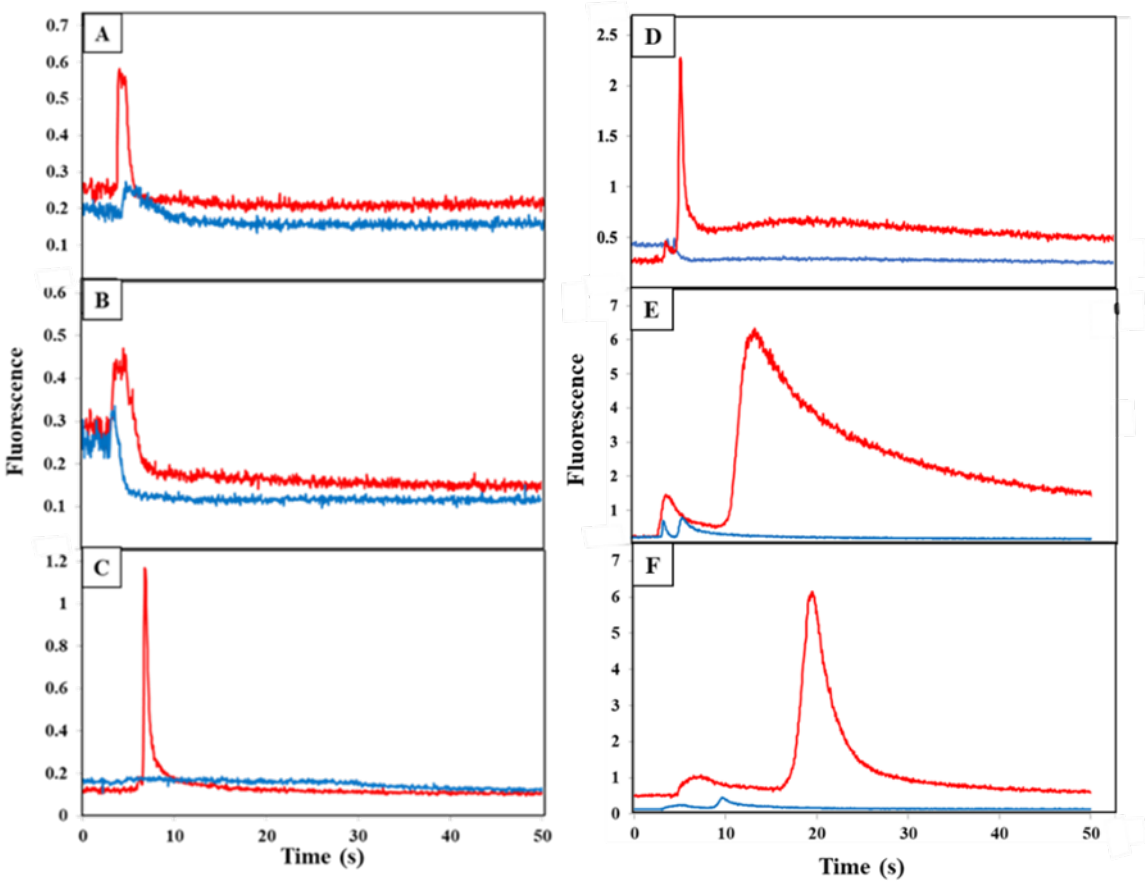

Figure 4.5 Fluorescence during elution after extraction of labeled PTB biomarkers from their respective single-antibody-modified columns (red) or a control monolith lacking attached antibody (blue) for (A, D) 100 nM CRF; (B, E) 30 nM TNF; and (C, F) 60 nM TAT in either (A-C) buffer or (D-F) depleted human blood serum.

Cross reactivity of each of the PTB biomarkers with off-target antibodies was tested as shown in Figure 4.6 for fluorescence during elution from a column with the two off-target antibodies for each biomarker, which was loaded from buffer. A small increase in the fluorescence was seen for both the antibody and blocked column, which possibly resulted from limited, nonspecific adsorption of each biomarker on the affinity column. These data clearly confirm that there is little cross reactivity occurring between each biomarker and the other two off-target antibodies.

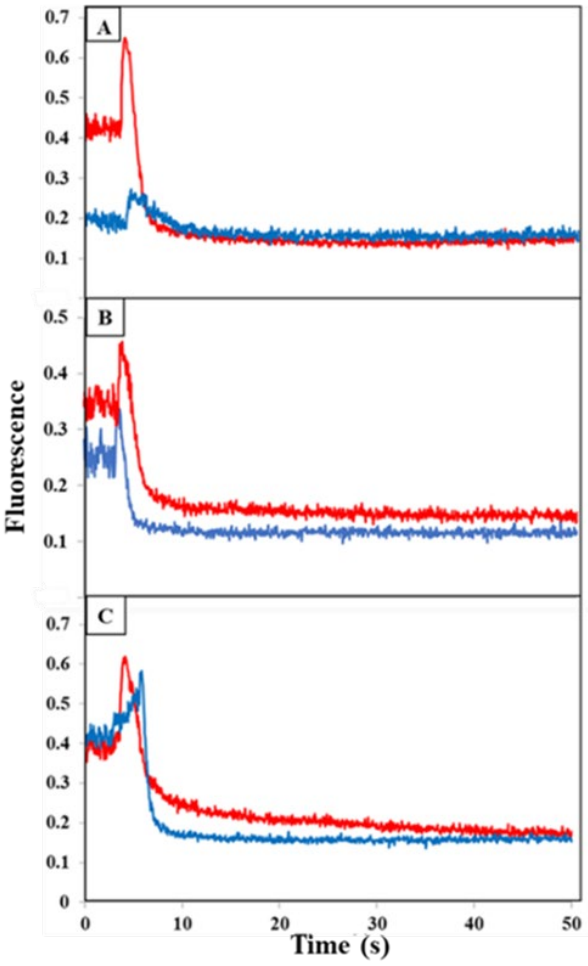

Figure 4.6 Fluorescence during elution after extraction from buffer on an off-target multiplexed affinity monolith (red) or a control monolith lacking attached antibodies (blue). Labeled (A) 100 nM CRF on anti-TNF and anti-TAT; (B) 30 nM TNF on anti-CRF and anti-TAT; (C) 60 nM TAT on anti-CRF and anti-TNF.

I then tested extraction of individual PTB biomarkers spiked into human blood serum on multiplexed antibody columns. As can be seen in Figure 4.7 small, narrow peaks were detected between 5-10 s for the blocked monoliths, which likely resulted from limited adsorption of the biomarker to the blocked column. However, a large peak in the fluorescence was observed at 5-10 s when each biomarker was eluted after extraction on a multiplexed antibody column. The peak appearances were also similar to when they were run on a single-antibody column in Figure 4.5. These results show the ability to individually extract CRF, TNF, and TAT on multiplexed antibody columns. I hypothesized that the most abundant proteins in serum might facilitate this nonspecific interaction, so I used five-fold diluted serum that had been depleted of abundant proteins in multiplexed studies.

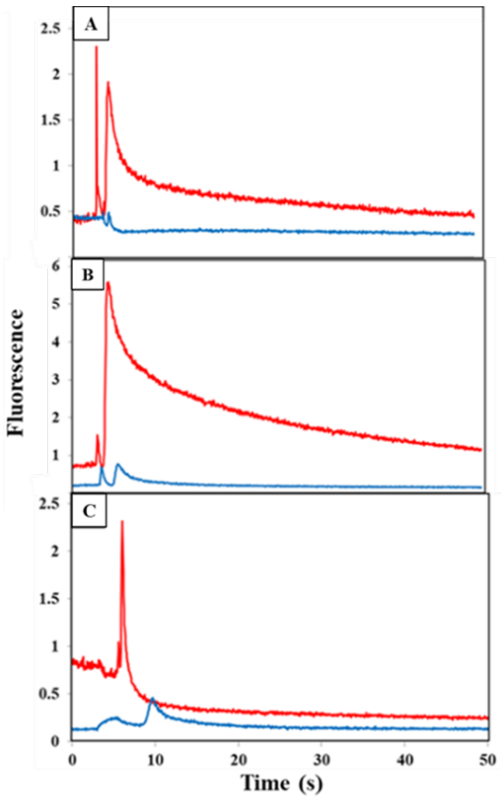

Figure 4.7 Fluorescence during elution of a single PTB biomarker loaded from depleted human serum and eluted from a multiplexed anti-CRF, anti-TNF, and anti-TAT monolith (red) or a control monolith lacking attached antibodies (blue). (A) 100 nM CRF, (B) 30 nM TNF, and (C) 60 nM TAT.

When I tested the individual protein biomarkers TNF and TAT, spiked into serum diluted 5-fold and loaded on blocked column, only a small elution peak was observed as seen in Figure 4.8A-B. This indicates that similar to the result in Figure 4.7B-C neither TNF nor TAT interacted significantly with the blocked column, even in the serum matrix that had not been depleted of abundant proteins. In contrast, a much larger elution peak was observed when both TNF and TAT were spiked into diluted blood serum and loaded on a blocked column as seen in Figure 4.8C. This result indicates some sort of combined interaction between TNF and TAT and components in blood serum, even on a blocked column. I hypothesized that the most abundant proteins in serum might facilitate this nonspecific interaction, so I used five-fold diluted serum that had been depleted of abundant proteins for multiplexing experiments.

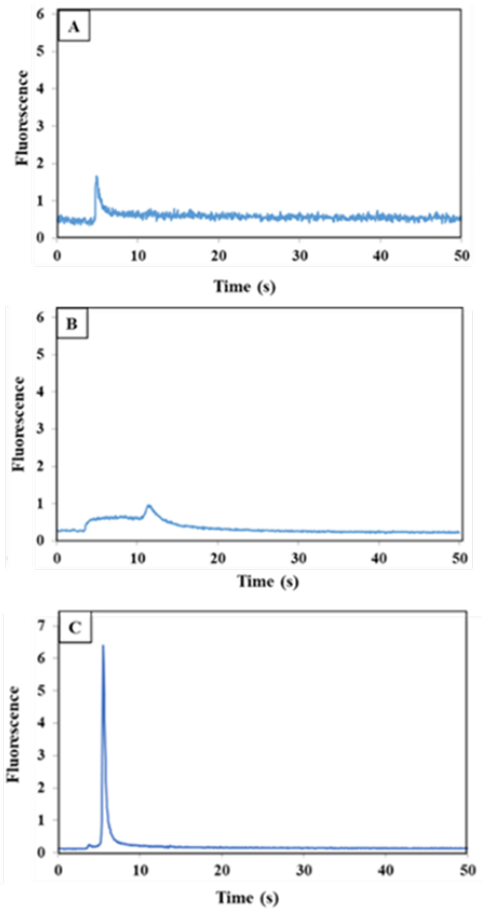

Figure 4.8 Fluorescence during elution after extraction of labeled (A) 30 nM TNF, (B) 60 nM TAT and (C) TNF (30 nM) and TAT (60 nM) from five-fold diluted human blood serum using a control monolith lacking attached antibodies (blue).

I studied the retention and elution from a combined anti-CRF, anti-TNF, and anti-TAT monolith by running a mixture of CRF, TNF, and nM TAT on either a multiplexed antibody column or a blocked column. Figure 4.9A shows an increase in the fluorescence signal during elution of all three biomarkers loaded from buffer on a combined anti-CRF, anti-TNF, and anti-TAT column as compared to a blocked column. The elution peak appeared at 7 s and was taller and wider than the peak from the blocked column. These data indicate successful retention and elution of these three PTB biomarkers in buffer using a multiplexed antibody column.

A similar experiment was performed wherein the biomarkers were spiked into depleted blood serum and loaded, and then eluted as seen in Figure 4.9B. An elution peak was observed initially at 5 s with a second, broader peak starting at 10 s. In contrast, a much smaller peak appeared at 5 s and the signal quickly went back to the baseline in the control experiment. This contrast with the large peak seen in Figure 4.8C supports the idea that the abundant serum proteins were responsible for the nonspecific binding observed in multiplexing experiments in serum when those proteins had not been removed. These results confirm successful retention and elution of these PTB biomarkers from a multiplexed monolith compared to a column lacking antibodies in a 3D printed device. These results also show promise for future extension to working with all nine PTB biomarkers on a single multiplexed antibody column.

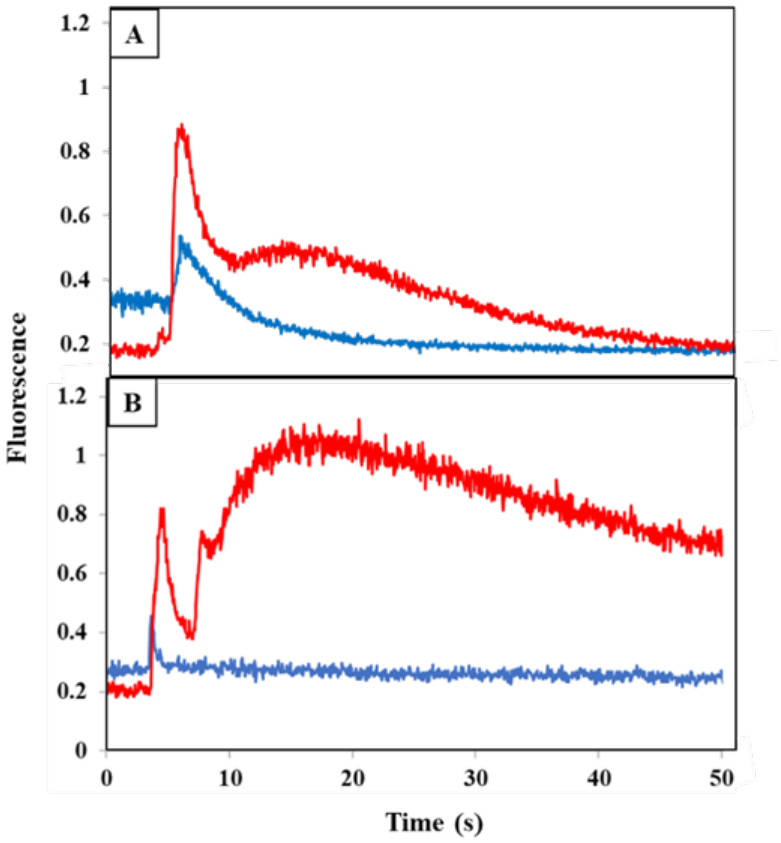

Figure 4.9 Fluorescence during elution after extraction on a combined anti-CRF, anti-TNF, and anti-TAT monolith (red) or a control monolith lacking attached antibodies (blue) for a mixture of labeled 100 nM CRF, 30 nM TNF, and 60 nM TAT from (A) buffer and (B) depleted human blood serum.

Further confirmation of the selective retention and elution of PTB biomarkers on a multiplexed immunoaffinity monolith is found in Figure 4.10. I took fluorescence images of a monolith after loading, rinsing, and elution of these three PTB biomarkers in depleted human blood serum on multiplexed immunoaffinity columns. The background-subtracted fluorescence seen in Figure 4.10 demonstrates that after the biomarker mixture was first loaded into a column, the fluorescence signal was at its highest. The control columns showed a drop in signal after rinsing to remove any nonspecifically bound analyte, indicating that the biomarkers were not strongly retained on blocked columns. However, the fluorescence signal was considerably higher after the rinsing step for antibody columns, showing specific retention of the biomarkers on multiplexed affinity monoliths compared to control columns. The signal on the monolith dropped more than twofold (with a p value of 0.14) after elution from the antibody columns, indicating some removal of retained PTB biomarkers. Elution from the control columns led to a small decrease in the already near background signal (with a p value of 0.28). In this initial evaluation the p values for the difference in signal after elution are not statistically significant, either for the control or antibody experiment. These data show limited biomarker retention for the control columns, with considerably more retention and elution of the biomarkers on the antibody columns, further supporting the use of these multiplexed immunoaffinity columns for PTB biomarker sample preparation.

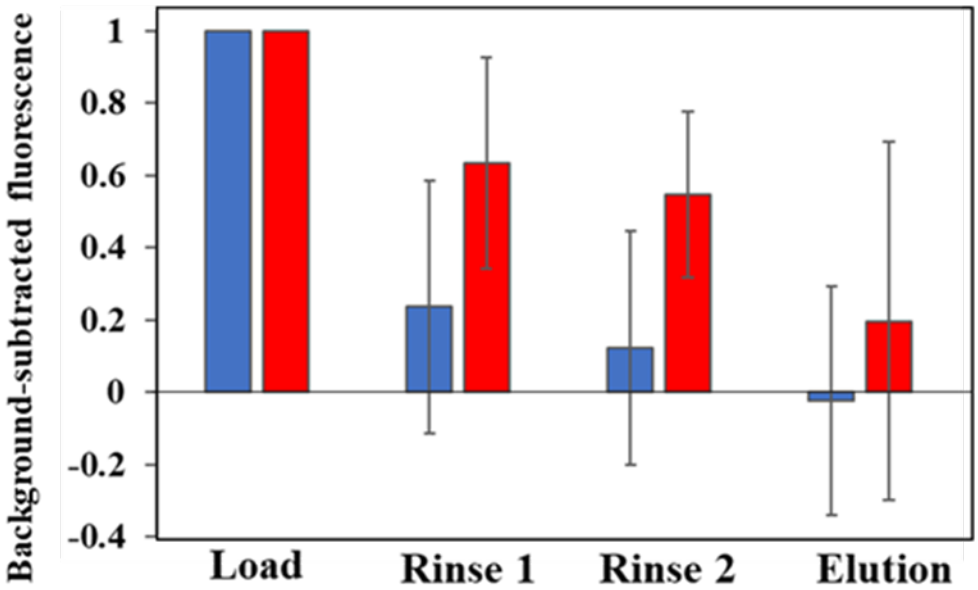

Figure 4.10 Normalized fluorescence signal on a monolith during the extraction of a mixture of 300 nM CRF, 90 nM TNF, and 180 nM TAT spiked into depleted human blood serum. (Blue) control monolith without attached antibodies; (red) monolith with attached antibodies. Error bars show the standard deviation for four replicates. No error bars are given for the loading data because they were normalized to 1.

I was able to extract CRF spiked into human blood serum with an antibody having moderate affinity (see Table 4.1). However, extraction of native CRF from human blood serum may require an antibody with higher affinity binding compared to the current one. In contrast, TAT has high affinity toward anti-TAT, and with a PTB risk level of ~5 μM,[8] I should readily be able to extract TAT from blood serum at clinical levels.

4.4 Conclusion

To improve sample preparation for analysis of biomarkers for maternal and fetal wellness, I created 3D printed microfluidic devices with multiplexed immunoaffinity monoliths. I characterized antibodies to target three PTB biomarkers. I also verified attachment of these antibodies to immunoaffinity columns using fluorescent imaging. Furthermore, I demonstrated

successful retention and elution of individual PTB biomarkers on single-antibody columns from both buffer and depleted human blood serum. Minimal cross reactivity was observed between each biomarker and the two off-target antibodies. Each of the three individual biomarkers were successfully extracted from multiplexed antibody columns. Finally, I demonstrated selective retention and elution of three PTB biomarkers on a multiplexed immunoaffinity column. In the future, I plan to multiplex additional antibodies on these columns, which should allow extraction of the whole panel of nine PTB biomarkers using a single immunoaffinity column. Additionally, these immunoaffinity monoliths form a significant part of a potential integrated chip that could be used in point-of-care in early identification of the risk of preterm birth.

4.5 References

1. Platchek, M.; Lu, Q.; Tran, H.; Xie, W. Comparative Analysis of Multiple Immunoassays for Cytokine Profiling in Drug Discovery. *SLAS Discov.* **2020,** *25*, 1197-1213.

2. Mori, A.; Saito, T.; Takahashi, M.; Shibata, M.; Tsuji, G.; Hatachi, S.; Takahashi, S.; Kumagai, S. Presence of anti-nuclear antibodies is a risk factor for the appearance of anti-drug antibodies during infliximab or adalimumab therapy in patients with rheumatoid arthritis. *PLoS One.* **2020,** *15*, e0243729.

3. Furuya, H.; Tabula, L.; Lee, R.; Kralovec, P.; Ramsden, M.; Wong, R.; Rosser, C. J. Analytical validation of ONCURIA a multiplex bead-based immunoassay for the non-invasive bladder cancer detection. *Pract. Lab. Med.* **2020,** *22*, e00189.

4. Mitchell, K.R.; Esene, J. E.; Woolley, A.T. Advances in Multiplex Electrical and Optical Detection of Biomarkers using Microfluidic Devices. *Anal. Bioanal.Chem.* accepted for publication (**2021**).

5. Souza, R.T.; McKenzie, E.J.; Jones, B.; de Seymour, J.V.; Thomas, M.M.; Zarate, E.; Han, T.L.; McCowan, L.; Sulek, K.; Villas-Boas, S.; Kenny L.C.; Cecatti, J.G.; Baker, P.N. Trace biomarkers associated with spontaneous preterm birth from the maternal serum metabolome of asymptomatic nulliparous women - parallel case-control studies from the SCOPE cohort. *Sci. Rep*. **2019,** *23*, *9*,13701

6. Hill,P.G., The measurment of albumin in serum and plasma. *Ann. Clin. Biochem.* **1985**, *22*, 565-578.

7. Polaskova, V.; Kapur, A.; Khan, A.; Molloy, M. P.; Baker, M. S. High-abundance protein depletion: comparison of methods for human plasma biomarker discovery. *Electrophoresis.* **2010,** *31*, 471-82.

8. Esplin, M. S.; Merrell, K.; Goldenberg, R.; Lai, Y.; Iams, J. D.; Mercer, B.; Spong, C. Y.; Miodovnik, M.; Simhan, H. N.; van Dorsten, P.; Dombrowski, M. Proteomic identification of serum peptides predicting subsequent spontaneous preterm birth. *Am. J. Obstet. Gynecol.* **2011,** *204*, 391 e1-8.

9. Knob, R.; Sahore, V.; Sonker, M.; Woolley, A. T. Advances in monoliths and related porous materials for microfluidics. *Biomicrofluidics.* **2016,** *10*, 032901.

10. Svec, F.; Lv, Y., Advances and recent trends in the field of monolithic columns for chromatography. *Anal. Chem.* **2015,** *87*, 250-73.

11. Andelkovic, U.; Tufegdzic, S.; Milica, P. Use of monolithic supports for high-throughput protein and peptide separation in proteomics. *Electrophoresis.* **2017,** *38*, 2851-2869.

12. Parker, E. K.; Nielsen, A. V.; Beauchamp, M. J.; Almughamsi, H. M.; Nielsen, J. B.; Sonker, M.; Gong, H.; Nordin, G. P.; Woolley, A. T. 3D printed microfluidic devices with immunoaffinity monoliths for extraction of preterm birth biomarkers. *Anal. Bioanal. Chem.* **2019,** *411*, 5405-5413.

13. Sonker, M.; Parker, E. K.; Nielsen, A. V.; Sahore, V.; Woolley, A. T. Electrokinetically operated microfluidic devices for integrated immunoaffinity monolith extraction and electrophoretic separation of preterm birth biomarkers. *Analyst.* **2017,** *143*, 224-231.

14. Abdiche, Y.; Malashock, D.; Pinkerton, A.; Pons, J. Determining kinetics and affinities of protein interactions using a parallel real-time label-free biosensor, the Octet. *Anal. Biochem.* **2008,** *377*, 209-17.

15. Estep, P.; Reid, F.; Nauman, C.; Liu, Y.; Sun, T.; Sun, J.; Xu, Y. High throughput solution-based measurement of antibody-antigen affinity and epitope binning. *MAbs.* **2013,** *5*, 270-8.

16. Nielsen, J. B.; Hanson, R. L.; Almughamsi, H. M.; Pang, C.; Fish, T. R.; Woolley, A. T. Microfluidics: Innovations in Materials and Their Fabrication and Functionalization. *Anal. Chem.* **2020,** *92*, 150-168.

17. Pandey, C. M.; Augustine, S.; Kumar, S.; Kumar, S.; Nara, S.; Srivastava, S.; Malhotra, B. D., Microfluidics Based Point-of-Care Diagnostics. *Biotechnol. J.* **2018,** *13*, 1700047.

18. Nielsen, A. V.; Beauchamp, M. J.; Nordin, G. P.; Woolley, A. T. 3D Printed Microfluidics. *Annu. Rev. Anal. Chem.* **2020,** *13*, 45-65.

19. Bickham, A. V.; Pang, C.; George, B. Q.; Topham, D. J.; Nielsen, J. B.; Nordin, G. P.; Woolley, A. T. 3D Printed Microfluidic Devices for Solid-Phase Extraction and On-Chip Fluorescent Labeling of Preterm Birth Risk Biomarkers. *Anal. Chem.* **2020,** *92*, 12322-12329.

20. Gong, H.; Beauchamp, M.; Perry, S.; Woolley, A. T.; Nordin, G. P. Optical Approach to Resin Formulation for 3D Printed Microfluidics. *RSC Adv.* **2015,** *5*, 106621-106632.

21. Costa, B.M.C.; Coelho, A.G.; Beauchamp, M.J.; Nielsen, G.B.; Nordin, G.P.; Woolley, A. T.; da Silva, J.A.F. 3D-printed Microchip Electrophoresis Device Containing Spiral Electrodes for Integrated Capacitively Coupled Contactless Conductivity Detection. *Anal.Bioanal.Chem*. **2021**, DOI:10.1007/s00216-021-03494-2.

22. Dincer, C.; Bruch, R.; Kling, A.; Dittrich, P. S.; Urban, G. A. Multiplexed Point-of-Care Testing - xPOCT. *Trends. Biotechnol.* **2017,** *35*, 728-742.

23. Gong, H.; Bickham B.P.; Woolley, A.T.; Nordin, G.P. Custom 3D printer and resin for 18 μm × 20 μm microfluidic flow channels. *Lab Chip.* **2017,** *17*, 2899-2909

24. Nielsen, J. B.; Nielsen, A. V.; Carson, R. H.; Lin, H. L.; Hanson, R. L.; Sonker, M.; Mortensen, D. N.; Price, J. C.; Woolley, A. T. Analysis of thrombin-antithrombin complex

formation using microchip electrophoresis and mass spectrometry. *Electrophoresis* **2019,** *40*, 2853-2859.

5. CONCLUSIONS AND FUTURE WORK

5.1 Conclusions

The focus of this dissertation is to develop immunoaffinity extraction methods for preterm birth biomarkers in human blood serum using 3D printed microfluidic devices. I was able to develop immunoaffinity columns for six of the nine PTB biomarkers, laying the foundation to simultaneously extract multiple PTB biomarkers in these systems. My work forms part of a larger effort to rapidly analyze the panel of nine PTB biomarkers with low cost to provide a way for doctors to predict risk for early labor.

5.1.1 Immunoaffinity Monoliths for PTB Peptide Extraction from Blood Serum

I developed immunoaffinity monoliths in 3D printed microfluidic devices, building on one developed by Parker et al.,[1] and designed to extract and elute a PTB peptide, corticotropin releasing factor, from spiked blood serum as described in chapter 2. This was the first demonstration of an immunoaffinity column in a 3D-printed device for the extraction of a peptide biomarker.

5.1.2 Antibody Characterization and Immunoaffinity Extraction of PTB Biomarkers

To support of my goal to develop immunoaffinity extraction of PTB biomarkers in 3D printed microfluidic devices, I characterized polyclonal and monoclonal antibodies toward PTB biomarkers in chapter 3. This characterization is necessary to identify appropriate antibodies for all nine PTB biomarkers for future retention and elution of mixtures of PTB biomarkers on immunoaffinity columns. Affinity binding between antigen and antibody was also studied to determine the strength of the binding between each biomarker toward its antibody, in support of subsequent multiplex experiments. I used polyclonal antibodies to target peptide 2, peptide 3, and lactoferrin. When I combined lactoferrin, ferritin[1] and CRF, I found that the polyclonal antibodies

were not specific to just the target biomarkers, and this off-target binding made polyclonal antibodies a less desirable option for future experiments. To overcome the cross reactivity issue with polyclonal antibodies, I evaluated monoclonal antibodies and was able to significantly reduce off-target binding between PTB protein biomarkers and non-target antibodies. Using monoclonal antibodies, I was able to demonstrate the immunoaffinity extraction of three PTB biomarkers: ferritin and lactoferrin from buffer, and peptide 2 from both buffer and blood serum.

5.1.3 Immunoaffinity Extraction of Multiplexed PTB Biomarkers

I optimized experimental conditions and obtained successful multiplexed retention and elution of three PTB biomarkers from both buffer and depleted human blood serum as described in chapter 4. An immunoaffinity monolith was formed inside 3D printed microfluidic devices via UV polymerization. Attachment of antibodies to the monolith and the absence of cross reactivity between PTB biomarkers and non-target antibodies were demonstrated. Equilibrium dissociation constant values for three PTB biomarkers toward their monoclonal antibodies were determined. A mixture of three monoclonal antibodies was immobilized on a monolith to enrich corticotropin releasing factor, tumor necrosis factor-α receptor type 1, and thrombin-antithrombin. Fluorescence on the column was measured to observe successful retention and elution of the three PTB biomarkers. This work shows important progress toward developing monoliths that can selectively extract all nine PTB biomarkers from human blood serum as a part of a complete diagnostic system.

5.2 FUTURE WORK

Antibody characterization was done for seven of the nine PTB biomarkers, but remains to be completed for peptide 1 and defensins. Defensins constitute a group of peptides, and at present it is not known which defensins are correlated to PTB risk. Future work on mass spectrometry

could determine which defensins should be included in the PTB biomarker panel. Although the dissociation constants for three PTB biomarkers were reported in this dissertation, the K_d values for the remaining six monoclonal antibodies need to be determined. A lack of nonspecific binding was observed between five PTB biomarkers and off-target monoclonal antibodies, but the interaction between the remaining PTB biomarkers toward off-target antibodies needs to be determined for eventual successful extraction of all nine PTB biomarkers. Additionally, an off-chip sample preparation step was done to separate PTB biomarkers from abundant proteins in serum. Finally, immunoaffinity extraction has been shown for four PTB biomarkers in blood serum; however, extraction of the remaining five PTB biomarkers from blood serum needs to be demonstrated. The development of an immunoaffinity column to combine the entire panel of the PTB biomarkers may need optimization of conditions including buffer pH, ionic strength, salt additive, and composition.

As described in this dissertation, I achieved successful retention and elution of many PTB biomarkers in immunoaffinity columns; however, I did all experimental steps of loading, rinsing, and elution manually. Collaborators in Dr. Nordin's lab have shown that pumps and valves can be 3D printed in microfluidic devices;[2-3] adding these components to my design could improve devices by allowing automatic extraction of PTB biomarkers. Adding pumps and valves to the design will also facilitate transferring analyte from the immunoaffinity column to other 3D printed analysis components.

The fabrication process could be improved by creating a 3D printed cover to place in the reservoir to prevent liquid from evaporating during the overnight incubation step and keep the channel wet to prevent bubbles from forming inside the channel. Multiple monoliths could be added to the current design to purify the PTB biomarkers in multiple groups based on different

extraction conditions. I could also add multiple inlet channels to the current design, controlled by valves for solvent switching, to allow consistent flow and automated extraction of multiple PTB biomarkers.

The long term goal of this work is to create 3D printed microfluidic devices containing three modules: immunoaffinity extraction, solid phase extraction and fluorescent labeling, and electrophoresis separation. In this dissertation I focused on the immunoaffinity extraction portion and demonstrated the extraction of multiple biomarkers from human blood serum using an immunoaffinity column. Next, it is necessary to integrate the immunoaffinity module with on-chip labeling and then with downstream separation. This will allow researchers to rapidly quantify the entire panel of PTB biomarkers from human blood serum as a part of a PTB risk analysis system. This work shows progress toward the long-term goal of assessing PTB and preventing early labor by development of immunoaffinity extraction of multiple PTB biomarkers from human blood serum. The 3D printed microfluidic devices used in this work are ideal for extraction of PTB biomarkers, and also show potential for use in detection of biomarkers for other diseases such as cancer.

5.3 References

1. Parker, E. K.; Nielsen, A. V.; Beauchamp, M. J.; Almughamsi, H. M.; Nielsen, J. B.; Sonker, M.; Gong, H.; Nordin, G. P.; Woolley, A. T. 3D printed microfluidic devices with immunoaffinity monoliths for extraction of preterm birth biomarkers. *Anal. Bioanal. Chem.* **2019,** *411*, 5405-5413.

2. Gong, H.; Woolley, A. T.; Nordin, G. P. 3D printed high density, reversible, chip-to-chip microfluidic interconnects. *Lab Chip.* **2018,** *18*, 639-647.

3. Gong, H.; Woolley, A. T.; Nordin, G. P. High density 3D printed microfluidic valves, pumps, and multiplexers. *Lab Chip.* **2016,** *16*, 2450-2458.